

## General Disclaimer

### One or more of the Following Statements may affect this Document

- This document has been reproduced from the best copy furnished by the organizational source. It is being released in the interest of making available as much information as possible.
- This document may contain data, which exceeds the sheet parameters. It was furnished in this condition by the organizational source and is the best copy available.
- This document may contain tone-on-tone or color graphs, charts and/or pictures, which have been reproduced in black and white.
- This document is paginated as submitted by the original source.
- Portions of this document are not fully legible due to the historical nature of some of the material. However, it is the best reproduction available from the original submission.

## Final Report

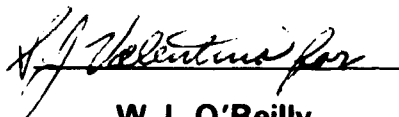
# BUFFER THERMAL ENERGY STORAGE FOR AN AIR BRAYTON SOLAR ENGINE

81-18087

August 31, 1981

Prepared by  
Hal J. Strumpf  
Kevin P. Barr

Approved by



W.J. O'Reilly  
Chief Engineer, Heat Transfer  
and Cryogenic Systems

Prepared for  
Jet Propulsion Laboratory  
California Institute of Technology  
Pasadena, California 91103



AIRESEARCH MANUFACTURING COMPANY

## FOREWORD

This report describes the results of a study conducted by AiResearch Manufacturing Company, a division of The Garrett Corporation, on the application of latent-heat buffer thermal energy storage to a point-focusing solar receiver equipped with an air Brayton engine. The study was performed for the Jet Propulsion Laboratory (JPL) under contract NAS 7-100/955136. The JPL contract monitor was Dr. Ram Manvi, Advanced Solar Thermal Technology Project.



AIRESEARCH MANUFACTURING COMPANY

81-18087  
Page ii

## ABSTRACT

This report summarizes the results of a study on the application of latent-heat buffer thermal energy storage to a point-focusing solar receiver equipped with an air Brayton engine. The AiResearch 65-kw(th) Air Brayton Solar Receiver and Mod "0" engine were used as a baseline system.

The operating life of a Brayton engine depends, in general, upon the number of start-stop cycles. The main advantage of buffer thermal energy storage is that it enables the engine to continue running during periods of cloud cover, thus reducing the number of engine shutdowns and increasing engine life.

To demonstrate the effect of buffer thermal energy storage on engine operation, a computer program was written for complete transient/steady-state Brayton cycle performance. The program models the recuperator, receiver, and thermal storage device as finite-element thermal masses; actual operating or predicted performance data are used for all components, including the rotating equipment.

The insolation input is minute-by-minute data recorded at the NASA/JPL test facility at Edwards Air Force Base for the year 1979. Based on this input and a specified control scheme, the computer program predicts the Brayton engine operation, including flows, temperatures, and pressures for the various components, along with the engine output power.

Because computer time considerations made it impractical to model an entire year's operation, a simulated year was developed. This involves grouping days with similar insolation patterns and selecting a representative day from each group. To determine the year's performance, the results from each of the representative days are multiplied by the number of days in the group, and all these products summed and normalized.

The simulated year was run for various weights of sodium chloride and lithium carbonate phase-change materials. The results indicate that thermal storage can afford a significant decrease in the number of engine shutdowns as compared to operating without thermal storage. It has also been found that the number of shutdowns does not continuously decrease as the storage material weight increases. In fact, there appears to be an optimum weight for minimizing the number of shutdowns. This is because of the sensible heat effects of the storage material. A large weight will not increase in temperature as rapidly as a small weight, given the same thermal input. This could result in lower cycle temperatures during a solar outage and cause an engine shutdown. Of course, too small a weight limits the storage capacity and increases the number of shutdowns.

An economic parametric study was performed to compare the cost of a thermal storage device with the savings in engine replacement afforded by the thermal storage. The study indicates that the economic viability of buffer thermal energy storage is largely a function of the achievable engine life. At low predicted life, thermal storage is economically attractive; for highly reliable, long-lived engines, thermal storage is not economical.



## ACKNOWLEDGMENTS

The authors of this report would like to acknowledge the significant contributions made to the study by Alan R. Hall.



## CONTENTS

<u>Section</u>		<u>Page</u>
1	INTRODUCTION	1-1
2	INSULATION DATA	2-1
3	BRAYTON ENGINE DEFINITION	3-1
	Computer Modeling	3-1
	System Operation	3-2
	Thermal Storage Flow Control	3-2
	Operating Conditions and Controls	3-2
	Electrical Energy Storage	3-6
4	BRAYTON ENGINE PERFORMANCE	4-1
5	THERMAL STORAGE DEVICE CONCEPTUAL DESIGN	5-1
6	ECONOMIC ANALYSIS	6-1
7	CONCLUSIONS AND RECOMMENDATIONS	7-1
	Conclusions	7-1
	Recommendations	7-1
<u>Appendix</u>		
A	SOLARBRAYTON COMPUTER PROGRAM	A-1
	General Method of Solution	A-1
	Computer Implementation	A-13
	Component Specifications	A-19
B	MOD "O" TURBOMACHINERY MAPS	B-1



## ILLUSTRATIONS

<u>Figure</u>		<u>Page</u>
1-1	Air Brayton Solar Engine Schematic	1-2
3-1	Thermal Storage and Receiver Flow Scheme	3-3
4-1	Insolation Input for April 7, 1979	4-10
4-2	Temperatures for April 7, 1979 (100 lb of NaCl)	4-11
4-3	Temperatures for April 7, 1979 (200 lb of NaCl)	4-12
4-4	Temperatures for April 7, 1979 (50 lb of Li <sub>2</sub> CO <sub>3</sub> )	4-13
4-5	Temperatures for April 7, 1979 (100 lb of Li <sub>2</sub> CO <sub>3</sub> )	4-14
4-6	Temperatures for April 7, 1979 (200 lb of Li <sub>2</sub> CO <sub>3</sub> )	4-15
4-7	Insolation Input for April 20, 1979	4-17
4-8	Temperatures for April 20, 1979 (200 lb of NaCl)	4-18
4-9	Temperatures for April 20, 1979 (200 lb of Li <sub>2</sub> CO <sub>3</sub> )	4-19
5-1	Conceptual Design of Thermal Storage Device (TSD)	5-2
6-1	Break-Even Cost for a 200-lb-NaCl TSD	6-3
A-1	Computer Model Schematic	A-3
A-2	Recuperator Model with Node Identification	A-7
A-3	Resistive Path Length	A-10
A-4	SOLARBRAYTON Subroutines Hierarchy Structure	A-14
A-5	Hierarchy Details for SOLARBRAYTON Component Subroutines	A-15
A-6	Flowchart for MAIN	A-17
A-7	Flowchart for TIMES	A-18
A-8	Sample Detailed Output	A-20
A-9	Sample One-Line Output	A-21
A-10	Integral Thermal Storage System	A-24



ILLUSTRATIONS (Continued)

<u>Figure</u>		<u>Page</u>
A-11	NonIntegral Thermal Storage System	A-25
A-12	Typical Shell and Tube Heat Exchanger Arrangement for Thermal Energy Storage	A-27

TABLES

<u>Table</u>		<u>Page</u>
2-1	Simulated Year Groupings for 1979 Edwards AFB Data	2-2
4-1	Thermophysical Properties of NaCl and Li <sub>2</sub> CO <sub>3</sub> at Melting Point	4-1
4-2	Simulated-Year Thermal Storage Summary	4-2
4-3	Performance Without Thermal Storage	4-2
4-4	Performance With 100 lb of NaCl at 1000°F Control Temperature	4-3
4-5	Performance With 200 lb of NaCl at 1000°F Control Temperature	4-4
4-6	Performance With 400 lb of NaCl at 1000°F Control Temperature	4-5
4-7	Performance With 200 lb of NaCl at 1300°F Control Temperature	4-6
4-8	Performance With 200 lb of Li <sub>2</sub> CO <sub>3</sub> at 1000°F Control Temperature	4-7
4-9	Thermal Storage Summary for April 7, 1979	4-9
A-1	Subroutine Identification List for SOLARBRAYTON Transient Performance Program	A-16





## NOMENCLATURE

A	Heat transfer area
ABSR	Air Brayton Solar Receiver
C	Thermal capacity
H	Convective coupling strength (thermal conductance)
h	Natural convection heat transfer coefficient
K	Conductive coupling strength
k	Thermal conductivity
L	Fusion capacity
ℓ	Resistive path length
M	Fraction liquid
NIP	Normal incident pyrheliometer
Nt	Turbomachinery speed
P, p	Pressure
PCM	Phase-change material
POWERE	Power output
Q, SUNINS	Insolation value
QFLUID	Heat absorbed by fluid
q	Net absorbed solar flux
R	Thermal resistance
T	Temperature
TC	Control temperature
TES	Thermal energy storage
TIT, T8	Turbine inlet temperature
TR	Desired temperature
TSD	Thermal storage device



NOMENCLATURE (Continued)

T15	Receiver outlet temperature
T16	TSD outlet temperature
t	Time
V	Capacity rate
W	Flow rate
X	Turbomachinery map reading parameter
Z	Overall coupling strength
Y	Specific heat ratio
$\Delta$	Difference
$\eta$	Adiabatic efficiency
$\theta$	$(Y-1)/Y$

Subscripts

c	Corrected
LM	Log mean
r	Ratio
s	Standard



## SECTION 1

### INTRODUCTION

This report summarizes the results of a study on the application of latent-heat buffer thermal energy storage (TES) to a point-focusing solar receiver equipped with an air Brayton engine. The main goal of the study was to establish the need, requirements, and size of buffer storage for a typical Brayton engine. Buffer storage is, by definition, of relatively low capacity, sufficient for keeping the engine running during brief periods of cloud cover (solar outages) but insufficient for long durations of low insolation.

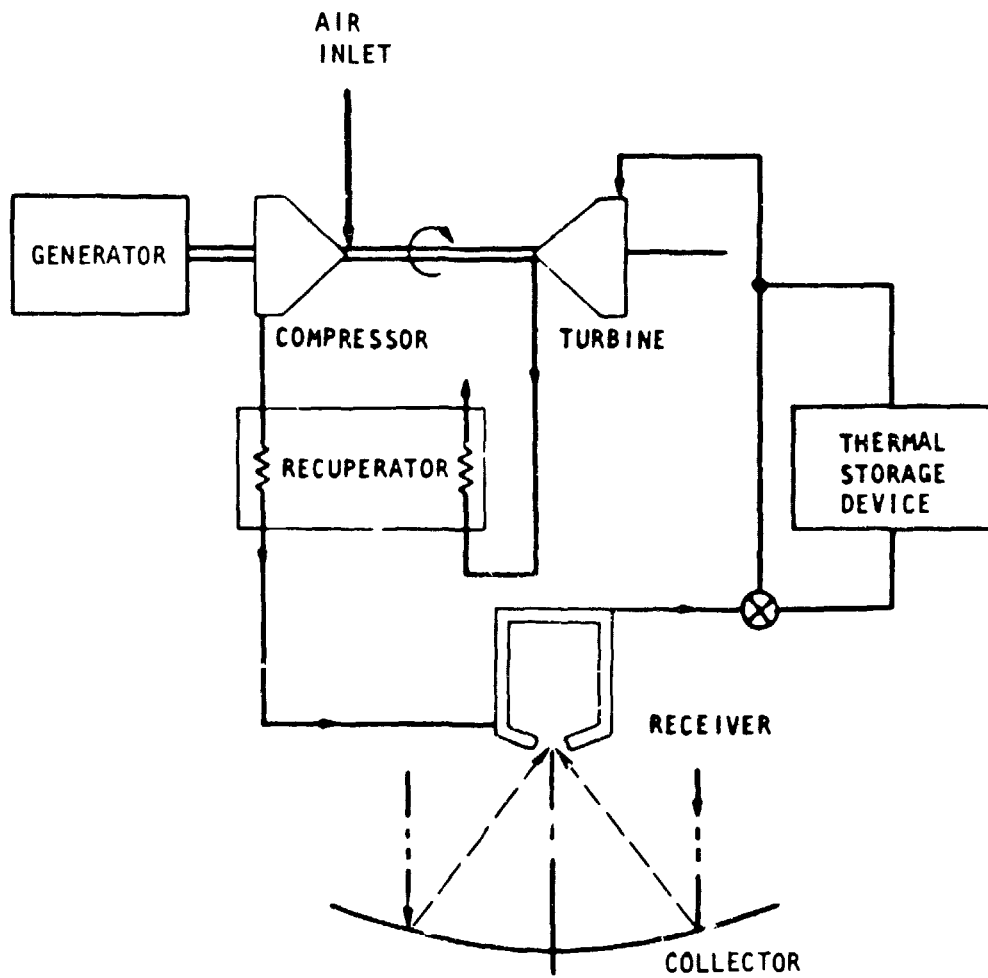
The AiResearch 85-kw(th) Air Brayton Solar Receiver (ABSR) and Mod "0" engine were used as the baseline system. The engine consists of a compressor, turbine, generator, and recuperator. The cycle is shown schematically in Figure 1-1. As can be seen, the cycle is "open"--ambient air is ingested by the compressor, picks up heat from the exhaust stream in the recuperator, absorbs the solar input in the receiver, is expanded in the turbine (producing the engine's power), and gives up heat to the incoming air before being exhausted to the environment. The thermal storage device (TSD) is also shown in Figure 1-1. The version of the Mod "0" engine used for the present study does not contain an auxiliary combustor for hybrid operation.

Depending upon the Brayton cycle pressure ratios and efficiencies, there is a minimum working fluid air temperature that must be supplied to the turbine to maintain cycle operation. During periods of solar outage, the primary heat source is removed or limited. The working fluid will initially extract heat from the thermal capacitance of the receiver and recuperator; but, after a time, additional energy must be supplied if the engine is to remain running.

A latent heat of fusion buffer TSD is investigated in this study. Energy is supplied to the cycle air from the latent heat released by the solidification of a phase-change material (PCM), which, in the temperature range of interest, will be an inorganic salt.

The main advantage of buffer TES is its ability to reduce the number of start-stop cycles required of the Brayton engine. For operation in a positive-net-power, self-sustaining mode, the power produced by the turbine must be greater than the power consumed by the compressor. This condition requires a reasonably high turbine inlet temperature (TIT). The thermal capacitance of the receiver, recuperator, and ducting is sufficient to maintain the necessary TIT for only a few minutes during a solar outage. The addition of thermal storage substantially increases the thermal capacitance of the system, resulting in an extension of the periods of solar outage during which the engine can remain running. Because many solar outages are of short duration, buffer TES can substantially reduce the number of engine shutdowns. With the operating life of the engine used in this application largely a function of the number of start-stop cycles, TES has the potential for increasing engine life and, hence, reducing engine yearly cost. Balanced against this is the cost of the TSD and its required auxiliary equipment.





A-17540-A

Figure 1-1. Air Brayton Solar Engine Schematic



To demonstrate the effect of buffer TES on engine operation, a complete transient/steady-state Brayton cycle performance computer program was written. The program models the recuperator, receiver, and TSD as finite-element thermal masses; all components, including the rotating equipment, utilize actual operating or predicted performance data. Writing this computer program and running the program for various conditions represented the major work effort of the study.



## SECTION 2

### INSOLATION DATA

For an analysis of the effect of buffer TES, the insolation distribution must be input. An idealized distribution was not assumed; rather, actual minute-by-minute insolation data were obtained from JPL for the NASA/JPL test facility at Edwards Air Force Base, California, for the entire year of 1979. The data, recorded on magnetic tape, are records from two Edwards AFB normal incident pyraheliometers (NIP) measuring local insolation in w/sq m. Data from NIP 2 are used for all months except for September and December, when technical malfunctions appear to have existed and the data from NIP 1 seem to be more reliable.

Because weather and insolation conditions vary over a year, a full year should be considered when analyzing the overall effect of TES. However, running 365 days on a transient computer program was considered excessively costly, especially when a number of thermal storage conditions are to be investigated. Therefore, the concept of a simulated year has been developed. Review of the data indicated that there were days with similar insolation patterns. For example, certain days had moderate clouds in the morning and were clear in the afternoon; other days were totally clear; etc. Days with similar insolation patterns were combined into groups, and a representative day selected from each group. A total of eleven groupings was formed. These are summarized in Table 2-1. Sunless days are days during which the engine is never turned on. As will be discussed in Section 3, this is equivalent to insolation always below 450 w/sq m.

Insolation data are available for 343 days out of the year. The remaining days had missing or obviously invalid data. To determine the year's performance, each representative day is run on the developed transient computer program, with the results from each day multiplied by the number of days in the group, and all these products summed. The sums are normalized to a full year by multiplying by 365/343.

The net heat input to the fluid in the receiver is assumed to be proportional to the insolation. The baseline conditions are a gross heat input of 85 kw(th) at an insolation value of 1000 w/sq m. At a cavity efficiency of 85 percent, this is equivalent to a net heat input of 72.25 kw(th). Thus, for any value of insolation,  $Q$ , the net heat input to the fluid is taken as  $72.25 \times Q/1000$  kw(th).



TABLE 2-1  
SIMULATED YEAR GROUPINGS FOR  
1979 EDWARDS AFB DATA

Type of Day	Number of Days	Representative Day
Clear	119	April 20
Minor afternoon clouds	11	September 9
Minor morning clouds	30	March 2
Heavy afternoon clouds	18	May 18
Heavy morning clouds	9	August 23
Thin clouds all day	27	April 26
Partly cloudy all day	18	June 3
Moderate clouds all day	44	February 21
Heavy clouds all day	32	April 7
Minimal clearing	24	January 17
Sunless	11	--
Total days	343*	

\*Remaining 22 days had missing or invalid data.



## SECTION 3

### BRAYTON ENGINE DEFINITION

#### COMPUTER MODELING

The computer program developed to analyze the air Brayton solar engine is described in Appendix A. This program, named SOLARBRAYTON, is a transient performance program that predicts the time-dependent behavior of the modeled system in response to the initial and boundary conditions. Some of the latter may be functions of time. The model contains control elements that modify system behavior according to the control logic and the values of certain performance indicators.

Two important points about the modeling are (1) that proper consideration has been given to the thermal capacity of the massive system components and to their effects on system time response and (2) that realistic performance specifications have been used for both the heat transfer components and the rotating equipment. The recuperator, receiver, and thermal storage device are each modeled using finite elements. The temperature change at each node during a time increment is calculated as a function of the local temperature gradients and the strengths of the various thermal couplings between the node in question and its neighboring nodes. The coupling strengths were determined from performance curves obtained from computer calculations of component performance over a range of flows and temperatures. The calculations were based on AiResearch experience with the heat transfer characteristics of the surfaces used for the components.

In this study the modeled run interval usually was one complete day from shortly after sunrise to sunset. Typical days were analyzed to give an indication of a simulated year's performance, as discussed in Section 2. For each typical day, separate computer runs were required for each of the combinations of the values of the various thermal storage and system control parameters used. This necessity to model numerous rather long time intervals, combined with the need to minimize the actual computer running time, dictated the level of modeling detail. The level chosen is detailed enough to provide fairly accurate and reliable results but simple enough to allow for the modeling of long time intervals without overly long computer running times.

Besides the true transient mode, SOLARBRAYTON has two other operating modes: steady-state and pseudo-transient. The steady-state option allows for rapidly obtaining the equilibrium solution of the system for a fixed set of boundary conditions. This is done by directly solving a set of simultaneous system equations and not by simply running the transient to steady-state. This option is especially useful in the early stages of the analysis to quickly provide initial insight into the system performance. Combining the other two modes gives the pseudo-transient mode, which provides a series of steady-state solutions as a function of changing boundary conditions. It was not used in the present study where rapidly changing boundary conditions are the rule rather than the exception and where true transient calculations are needed for trustworthy results. The discussion in Appendix A centers on the primary program mode, the transient performance prediction mode.





## SYSTEM OPERATION

### Thermal Storage Flow Control

As can be seen from the schematic in Figure 1-1, the TSD is located downstream of the receiver and upstream of turbine. Also shown is a valve that enables some or all of the flow through the receiver to bypass the TSD and go directly to the turbine. This flow control valve is an expensive piece of equipment, requiring three-way flow modulation, high temperature operation (up to 1500°F), and relatively large size (a 4-in. valve is necessary to limit pressure losses). Nevertheless, the valve is considered to be a necessary component. Removal of the valve would require the TSD to be in line with the receiver and turbine at all times. This presents an unacceptable penalty during a cold startup, when the entire engine (including the TSD) has to be heated to operating temperature from ambient or near ambient conditions. During such a startup the attainment of a self-sustaining TIT would be delayed while the TSD is heated. Motoring times of around 45 min would be required. This is considered to be excessive for the Mod "0" engine. In addition to the long motoring time, a large energy storage capacity would have to be made available through storage batteries or similar devices.

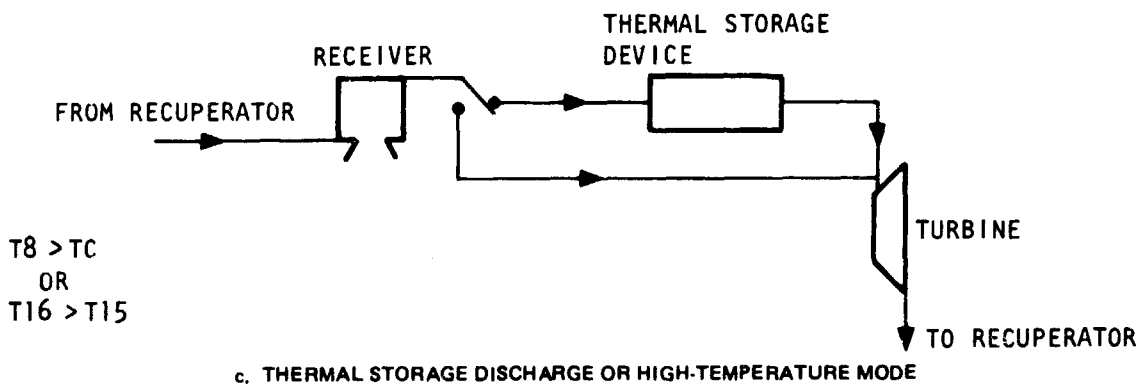
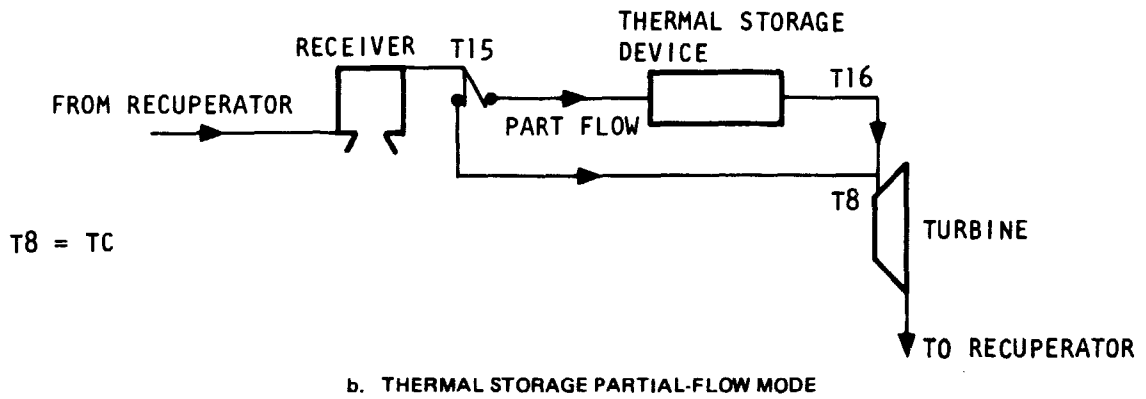
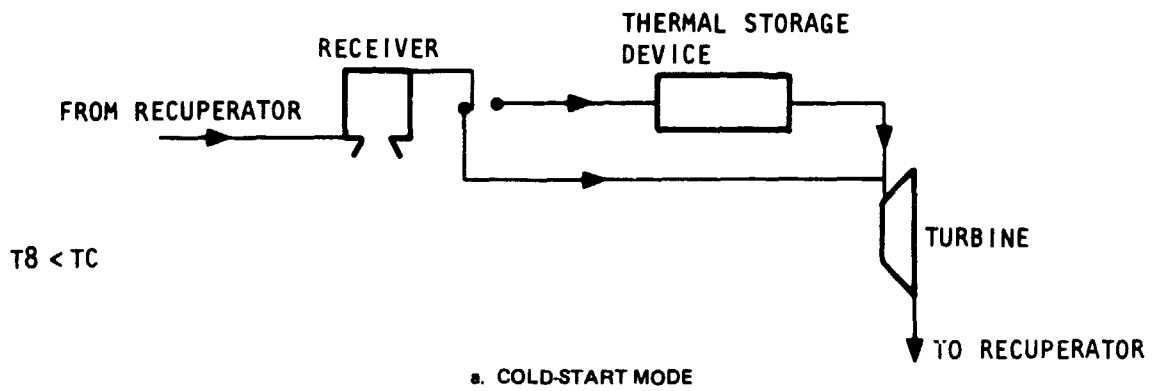
The flow control valve is used to modulate the flow rate through the TSD as a function of air temperature. The valve positions are illustrated in Figure 3-1: part a of the figure shows a complete bypassing of the TSD, b shows a partial flow through the device, and c shows full flow with the TSD in series with the receiver. The position of the modulating valve and, hence, the flow rate through the TSD, is determined by simple control logic keyed to a control temperature (TC). This logic, and its integration into the system operation, is described below.

### Operating Conditions and Controls

The operating conditions for the engine were selected after some preliminary study as representative of a reasonable operating approach. Budget restraints did not permit a complete optimization of the operating control approach, however. The controls are keyed to measurements of the cycle air temperature. Three temperature measurements are required, as indicated in Figure 3-1: receiver outlet temperature, T15; TSD outlet temperature, T16; and TIT, T8. An additional temperature measurement may be desirable at the recuperator hotside outlet (to monitor overheating of the recuperator), but the measurement does not enter directly into the control scheme. No temperature measurements are required in the PCM. Also required is a solar pyrheliometer to measure the local value of the insolation.

The measured temperatures control the position of the modulating valve and the speed of the rotating group. By the use of guide vanes and restricting orifices, the turbomachinery can be controlled so as to yield any set temperature in the system or to rotate at a given speed. A control box is required to orchestrate these functions. The control scheme is expected to be readily transferable to a real engine.





A-17631

Figure 3-1. Thermal Storage and Receiver Flow Scheme

At the start of each day, all components are assumed to be at ambient temperature (70°F). This is a conservative approach, because on some days temperatures may be somewhat above ambient (especially in the TSD). If a day-by-day year were run on the computer program and if there were no missing or invalid data, the actual component temperature levels could be computed. However, given the present simulated-year technique, assuming ambient conditions for all components would seem to be the most prudent approach. As will be discussed below, the system (including the TSD) is allowed to run itself down at the end of each day, so the components are relatively cool at shutdown. The approximate average component temperatures at shutdown are:

<u>Component</u>	<u>Temperature, °F</u>
Recuperator	500
Receiver	630
TSD	800 (completely solid)

The collector is assumed to be defocused at the beginning of the day, and remains so until the insolation reaches a minimum value, taken as 450 w/sq m. This value is sufficient for self-sustained engine operation at a power output of around 4 kw, and a cold startup motoring time of about 20 min, about the maximum desirable for the Mod "0" engine. Lower values of the startup insolation might result in excessive motoring times (if self-sustained operation can be attained at all). Higher values tend to waste some of the available solar energy.

As the collector is focused, the rotating group is turned on, using an auxiliary power supply to motor the engine at 53,000 rpm. The engine must be running any time the collector is focused, to prevent rapid overheating of the receiver. The fluid flow completely bypasses the TSD, as shown in Figure 3-1a. If during this motoring period the insolation drops below 400 w/sq m, the engine is shut off and the collector defocused. This is done to prevent useless motoring and draining of the auxiliary power supply. The collector is focused and the engine restarted when the insolation again reaches 450 w/sq m.

As the components heat up, the cycle air temperature increases until a net positive power is produced by the engine. This occurs at a TIT of around 800°F. As this point, the auxiliary power supply is disconnected. The engine continues to run with the rotating speed controlled at 53,000 rpm. Once the positive net power condition is attained, the engine is allowed to run until it shuts itself down; thus insulations below 400 w/sq m do not result in automatic shutdown. Any shutdown is accompanied by collector defocusing. The engine is always restarted (and the collector focused) when the insolation reaches 450 w/sq m. During temporary shutdowns, the recuperator, receiver, and TSD temperatures are assumed to be unchanged. This is a reasonable assumption because, with good insulation, shutdown durations of less than a half-hour will not result in much temperature change. Thus, once positive net power has been attained, any subsequent restarts on that day will require only an initial burst of power from the auxiliary source, because the fluid temperature conditions will almost immediately be self-sustaining.

As the engine runs and the solar insolation increases, the receiver and recuperator temperatures increase until the TIT (T8 in Figure 3-1) reaches the control temperature, TC. At this point partial flow is initiated through the TSD (Figure 3-1b). To limit the required flow range of the modulating valve, a minimum TSD flow equal to 10 percent of the receiver flow is assumed. This flow will immediately lower the TIT, so the TC should be chosen high enough that the engine will not turn off at this point. When the TIT again becomes equal to the TC, the flow rate through the TSD is increased so as to maintain this equality.

As the system continues to heat up, the TSD outlet temperature (T16) reaches the TC. At this point, all the receiver flow will be going through the TSD (Figure 3-1c). Further heating results in the TIT exceeding the TC. The engine has been running at 53,000 rpm all this time. When the receiver outlet temperature (T15) reaches 1500°F, the cycle control is switched so as to maintain this temperature; the speed is allowed to vary to effect this control. It should be noted that the receiver outlet temperature rather than the TIT is controlled. This protects the receiver from possible high temperatures because with the TSD in series (Figure 3-1c) a T8 of 1500°F could be accompanied by a considerably higher T15. The 1500°F air temperature limit is the design maximum for the ABSR.

As the insolation increases, the fluid flow rate (and hence, the engine speed) must increase so as not to exceed a 1500°F outlet temperature. Conversely, the speed decreases as the insolation drops. If the speed drops to as low as 53,000 rpm, this value is maintained and the temperature is no longer controlled. This minimum speed was selected to limit the recuperator hot-side inlet temperature to about 1200°F, the nominal limit for the Mod "0" design. Maintaining a TIT of 1500°F at speeds less than 53,000 rpm will result in excessive recuperator temperatures.

A continuing decrease in insolation will eventually result in T8 dropping below the TC. However, since T16 will be greater than T15, full flow is maintained through the TSD. The system continues in this mode until it shuts itself down. Any subsequent startups will occur with T16 greater than T15, so the full flow is routed through the TSD (Figure 3-1c).

Other control strategies are possible. For example, rather than controlling speed at lower levels of insolation, the TIT could be maintained at a value low enough to protect the recuperator. Also, the cold startup speed might possibly be reduced, because the temperatures are low during this phase. The turbine efficiency, however, tends to decrease at lower speeds. In addition, the lower speeds may result in mismatched conditions between the turbine and compressor, preventing a smooth startup.

Different strategies might also be employed for the TSD. For example, once the TSD were fully charged (PCM completely melted), the flow could bypass the TSD during high solar insolation periods. This would save pressure drop and increase cycle efficiency. Some flow would still be required, however, to overcome thermal losses to the environment.



A quite different flow scheme was considered and some sample runs made. The approach used low-level insolation (less than 450 w/sq m) at the beginning of the day to partially heat the TSD. Because it is not desirable to excessively motor the engine, an auxiliary flow loop was employed, using a separate compressor or fan to flow air through the receiver and TSD without running the engine. It appears that this approach has the potential to decrease the number of engine shutdowns while increasing the net energy produced. Also the engine startup power required is substantially reduced. However, in addition to the extra compressor, a number of three-way valves, including at least one expensive 1500°F valve, would be required. In addition, the energy required to operate the auxiliary compressor would have to be stored, requiring a large increase in storage battery capacity. It is felt that despite the potential advantages, the increased complexity and cost of this approach renders it impractical.

### Electrical Energy Storage

To start the Brayton engine and motor it until a self-sustaining fluid temperature is attained, energy must be supplied to the generator (acting as an alternator) from an auxiliary source. A reasonable source of this energy might be automotive type batteries. These batteries are typically rated at a maximum output of 200 amp at 12 v. This yields a maximum power of about 2.4 kw. The total usable storage capacity is 0.5 to 1.0 kwhr.

The engine requires a power of about 25 kw to motor at 53,000 rpm. The energy required to motor until self-sustaining conditions are reached is about 2 kwhr. Thus, the power requirement is more severe than the energy requirement, and 10 to 15 batteries would be necessary. The starting power might be reduced by motoring initially at a lower speed while the fluid heats up.

The startup energy required for a given day is charged to that day's output at an in-to-out efficiency of 50 percent. In other words, if 2 kwhr is required for startup, 4 kwhr is charged against the output. The overall 50-percent efficiency includes all losses (charging, discharging, rectifying, etc.).



## SECTION 4

### BRAYTON ENGINE PERFORMANCE

In accordance with the conditions discussed in Section 3, simulated years were run for various thermal storage materials, weights, and control temperatures (TC). Because of budget limitations, it was possible to run only six simulated years. Two PCM's were studied, sodium chloride (NaCl) and lithium carbonate (Li<sub>2</sub>CO<sub>3</sub>). The thermophysical properties assumed for the two salts are listed in Table 4-1.

TABLE 4-1

THERMOPHYSICAL PROPERTIES OF NaCl AND Li<sub>2</sub>CO<sub>3</sub> AT MELTING POINT

Parameter	NaCl	Li <sub>2</sub> CO <sub>3</sub>
Melting point, °F	1472	1333
Latent heat of fusion, Btu/lb	206	261
Solid heat capacity, Btu/lb-°F	0.260	0.630
Liquid heat capacity, Btu/lb-°F	0.274	0.600
Solid density, lb/cu ft	121.7	122
Liquid density, lb/cu ft	97.3	114
Solid thermal conductivity, Btu/hr-ft-°F	0.97	0.87
Liquid thermal conductivity, Btu/hr-ft-°F	0.58	1.16
Viscosity, lb/ft-hr	3.9	11.7
Coefficient of volumetric expansion, °F <sup>-1</sup>	$1.94 \times 10^{-4}$	$1.13 \times 10^{-4}$

A summary of the results is given in Table 4-2. In the table the net energy is the yearly energy output minus twice the yearly energy input (as discussed in Section 3). With the tube size and spacing constant, as discussed in Appendix A, the thermal storage device heat transfer area is proportional to the PCM weight. The heat exchangers are essentially identical for equal weights of NaCl and Li<sub>2</sub>CO<sub>3</sub>, a result of the similarity in solid density of the two substances.

The day-by-day results of the computer runs from which the simulated years were derived are given in Tables 4-3 through 4-8. As an example of the arithmetic used to establish the performance for the simulated year, consider the

TABLE 4-2

## SIMULATED-YEAR THERMAL STORAGE SUMMARY

PCM	PCM Weight, lb	TSD Heat Transfer Area, sq ft	Control Temperature, °F	Number of Shutdowns	Net Energy, kwhr
---	0	--	--	1,810	44,676
NaCl	100	22.76	1,000	1,202	41,983
NaCl	200	45.53	1,000	1,084	40,723
NaCl	400	91.06	1,000	1,318	38,310
NaCl	200	45.53	1,300	1,188	41,276
Li <sub>2</sub> CO <sub>3</sub>	200	45.53	1,000	1,276	37,138

TABLE 4-3

## PERFORMANCE WITHOUT THERMAL STORAGE

Representative Day	Number of Shutdowns	Energy Output, kwhr	Energy Input, kwhr
April 20	1	152.7	1.1
September 9	2	150.9	1.9
March 2	2	168.2	1.6
May 18	3	136.1	1.9
August 23	9	146.9	1.2
April 26	3	146.3	1.8
June 3	10	123.7	1.5
February 21	10	129.6	1.9
April 7	14	47.7	1.4
January 17	9	36.3	0.8



TABLE 4-4

PERFORMANCE WITH 100 LB OF NaCl AT 1000°F CONTROL TEMPERATURE

Representative Day	Number of Shutdowns	Energy Output, kwhr	Energy Input, kwhr
April 20	1	145.4	1.1
September 9	1	144.5	1.9
March 2	2	159.7	1.6
May 18	1	127.3	1.9
August 23	7	137.9	1.2
April 26	1	137.8	1.8
June 3	4	115.1	1.5
February 21	6	121.8	1.9
April 7	11	40.8	1.4
January 17	6	30.0	0.8





TABLE 4-5

PERFORMANCE WITH 200 LB OF NaCl AT 1000°F CONTROL TEMPERATURE

Representative Day	Number of Shutdowns	Energy Output, kwhr	Energy Input, kwhr
April 20	1	141.7	1.1
September 9	1	141.8	1.9
March 2	2	156.0	1.6
May 18	1	124.6	1.9
August 23	8	135.2	1.2
April 26	1	134.0	1.8
June 3	4	111.8	1.5
February 21	6	118.5	1.9
April 7	8	36.8	1.4
January 17	5	25.7	0.8



TABLE 4-6

PERFORMANCE WITH 400 LB OF NaCl AT 1000°F CONTROL TEMPERATURE

Representative Day	Number of Shutdowns	Energy Output, kwhr	Energy Input, kwhr
April 20	1	134.4	1.1
September 9	1	134.7	1.9
March 2	2	148.8	1.6
May 18	1	117.7	1.9
August 23	8	128.9	1.2
April 26	1	126.7	1.8
June 3	8	106.9	1.5
February 21	5	113.2	1.9
April 7	11	28.2	1.4
January 17	9	20.5	0.8



TABLE 4-7

PERFORMANCE WITH 200 LB OF NaCl AT 1300°F CONTROL TEMPERATURE

Representative Day	Number of Shutdowns	Energy Output, kwhr	Energy Input, kwhr
April 20	1	143.1	1.1
September 9	1	143.3	1.9
March 2	2	157.2	1.6
May 18	1	126.1	1.9
August 23	7	135.9	1.2
April 26	1	135.5	1.8
June 3	5	113.0	1.5
February 21	6	120.0	1.9
April 7	10	39.0	1.4
January 17	6	26.6	0.8



TABLE 4-8

PERFORMANCE WITH 200 LB OF  $\text{Li}_2\text{CO}_3$  AT 1000°F CONTROL TEMPERATURE

Representative Day	Number of Shutdowns	Energy Output, kwhr	Energy Input, kwhr
April 20	1	131.1	1.1
September 9	1	130.3	1.9
March 2	2	145.7	1.6
May 18	1	112.8	1.9
August 23	8	125.2	1.2
April 26	1	123.3	1.8
June 3	8	102.6	1.5
February 21	5	108.9	1.9
April 7	9	27.8	1.4
January 17	10	17.3	0.8



data for performance without thermal storage listed in Table 4-3 and its grouping distribution given in Table 2-1. The total number of unnormalized shutdowns for the year is:  $1 \times 119 + 2 \times 11 + 2 \times 30 + 3 \times 18 + 9 \times 9 + 3 \times 27 + 10 \times 18 + 10 \times 44 + 14 \times 32 + 9 \times 24 + 0 \times 11 = 1701$ . This is normalized to a complete year by:  $1701 \times (365/343) = 1810$ . The yearly energy output and input are calculated in the same manner.

All but one of the simulated years were for a TC of  $1000^{\circ}\text{F}$ . As previously discussed, from a cold startup this temperature must be attained at the receiver outlet before any flow is routed through the TSD (see Figure 3-1). Subsequently, the turbine inlet temperature is controlled to this value until the TSD is heated sufficiently to allow the TIT to rise with full flow passing through the TSD. The  $1000^{\circ}\text{F}$  TC is about as low as possible without causing a shutdown when the TSD flow is first initiated (and the TIT drops considerably from the TC). The one run at a higher TC ( $1300^{\circ}\text{F}$ ) did not result in improved performance; the slightly increased energy output was more than offset by an additional 100 shutdowns.

The simulated-year results in Table 4-2 indicate that thermal storage can produce a significant decrease in the number of shutdowns as compared to a system with no thermal storage (a 40-percent decrease in the case of 200 lb of NaCl at TC =  $1000^{\circ}\text{F}$ ). Whether this decrease, and the accompanying increase in engine life, is sufficient to pay for the thermal storage system will be discussed in Section 6.

From the first four entries in Table 4-2, it can be seen that the number of shutdowns does not continue to decrease as the PCM weight increases. This is because of the sensible heat effects of the PCM. The charging and discharging of the TSD involves a significant amount of sensible heating and cooling; indeed, the PCM is at ambient conditions at the start of a day, and the heat required to raise the temperature to the melting point is considerably greater than the latent heat for either PCM. A large PCM weight will not increase in temperature as rapidly as a small weight, given the same thermal input. This could result in a lower turbine inlet temperature during a solar outage and cause an engine shutdown. Of course, too small a PCM weight limits the storage capacity and may decrease the length of time the engine can remain running with reduced insolation.

A similar effect is noticeable when comparing equal weights of NaCl and  $\text{Li}_2\text{CO}_3$ . Since the  $\text{Li}_2\text{CO}_3$  has a solid heat capacity roughly two and one-half times that of the NaCl, the  $\text{Li}_2\text{CO}_3$  will not heat up as rapidly. This results in an increase in the number of shutdowns.

To further investigate this trend, 50- and 100-lb  $\text{Li}_2\text{CO}_3$  thermal storages (TC =  $1000^{\circ}\text{F}$ ) were run for the representative day of heavy clouds all day, April 7. The results, along with the previously run conditions for April 7, are presented in Table 4-9.



TABLE 4-9

## THERMAL STORAGE SUMMARY FOR APRIL 7, 1979

PCM	PCM Weight, lb	Number of Shutdowns	Net Energy, kwhr
--	0	14	44.9
NaCl	100	11	38.0
NaCl	200	8	34.0
NaCl	400	11	25.4
Li <sub>2</sub> CO <sub>3</sub>	50	9	37.3
Li <sub>2</sub> CO <sub>3</sub>	100	8	32.2
Li <sub>2</sub> CO <sub>3</sub>	200	9	25.0

It can perhaps be generalized from the results in Tables 4-9 and 4-2 that for given solar input conditions, any potential thermal storage PCM would have an optimum weight for minimizing the number of shutdowns: this interesting conclusion has not been apparent prior to the present work. Indeed, it was generally assumed that thermal storage performance improved as the PCM weight was increased.

On the other hand, the trend in net energy produced seems to be more straightforward: the energy decreases with increasing PCM weight. This is because it is assumed that the TSD cools to ambient temperature before the start of each day. Since the TSD shutdown temperature is about 800°F, a substantial amount of energy is lost each day, especially for a high heat capacity material such as Li<sub>2</sub>CO<sub>3</sub>. The additional energy produced as a result of the reduction in number of shutdowns is small, not nearly enough to overcome the TSD environmental losses.

In Appendix A, the plotting capabilities of the computer program are discussed. Figure 4-1 shows the insolation input for April 7, 1979. A very cloudy day is readily apparent. Two of the key outputs, turbine inlet temperature and TSD outlet temperature, are shown in Figures 4-2 through 4-5 for some of the conditions of Table 4-9.

From the 200-lb NaCl case as an example (Figure 4-3), the engine operating characteristics can be observed. It should be noted that during shutdown periods, the fluid temperatures are assumed to be constant. This reflects the assumption of negligible thermal losses. When the engine is first turned on, all the flow bypasses the TSD. When the TIT reaches the TC (at about 8.5 hr), flow is initiated through the TSD. This causes an immediate decrease in the TIT. It should be noted that there have already been two engine shutdowns to this point.



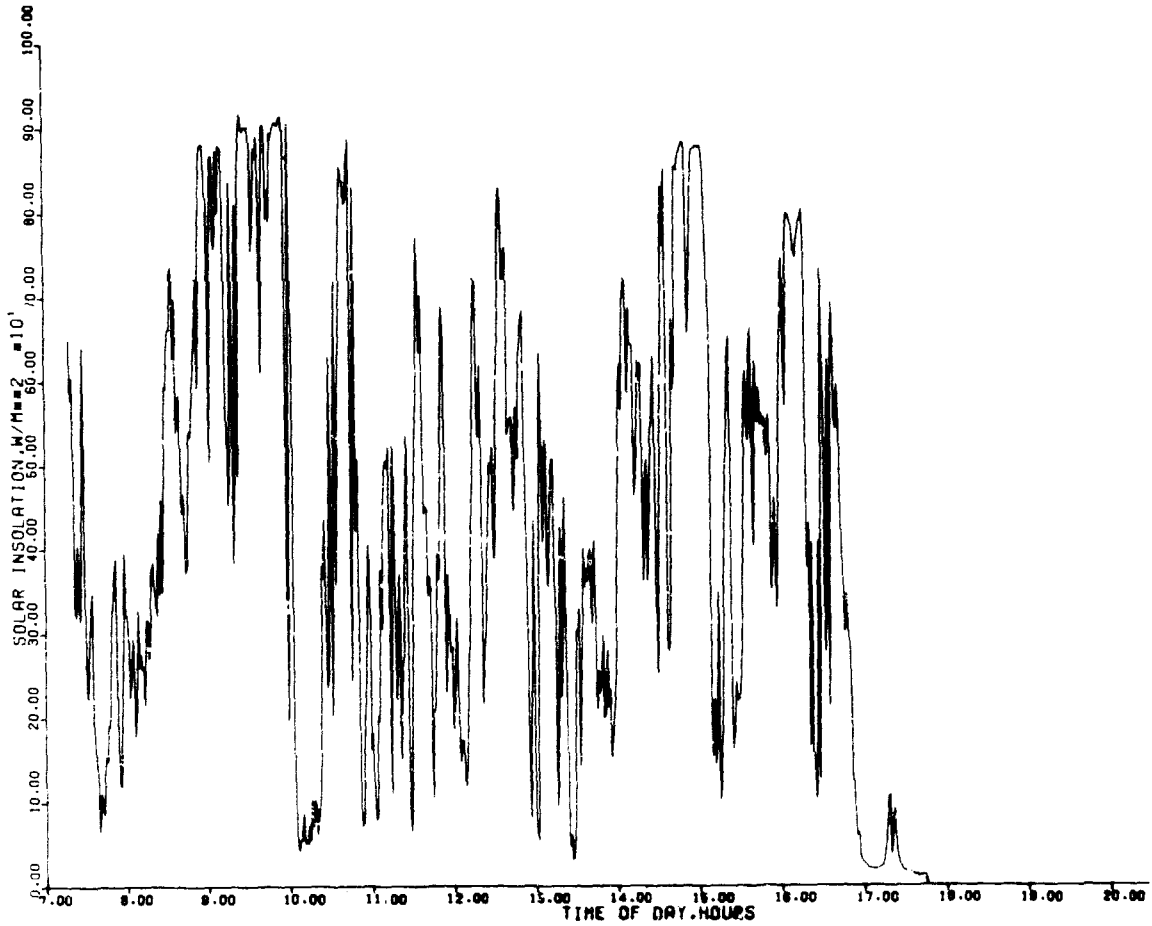
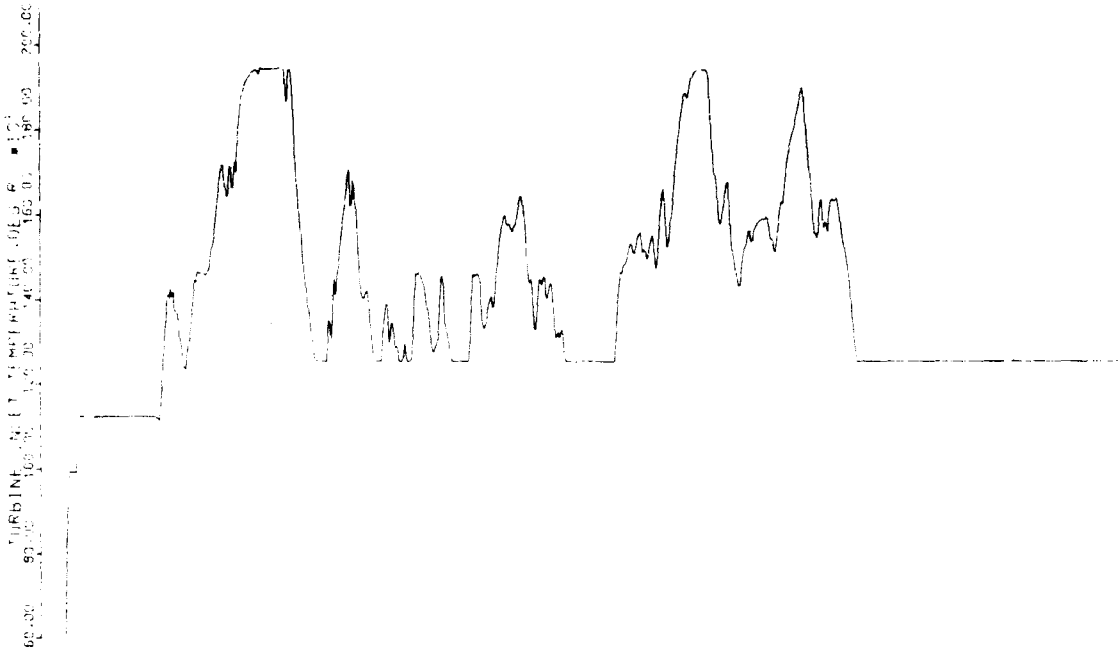


Figure 4-1. Insolation Input for April 7, 1979

A-17488

ORIGINAL PAGE IS  
OF POOR QUALITY



100 LB NACL (TC=1000 DEG F)

APRIL 7, 1979

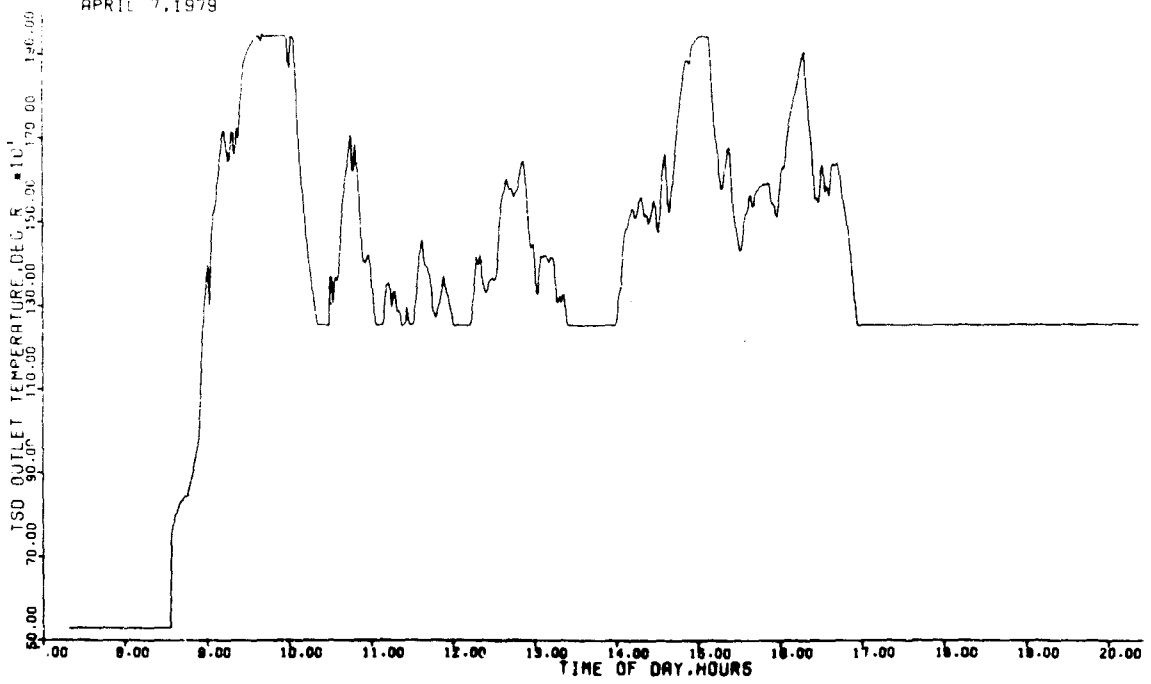
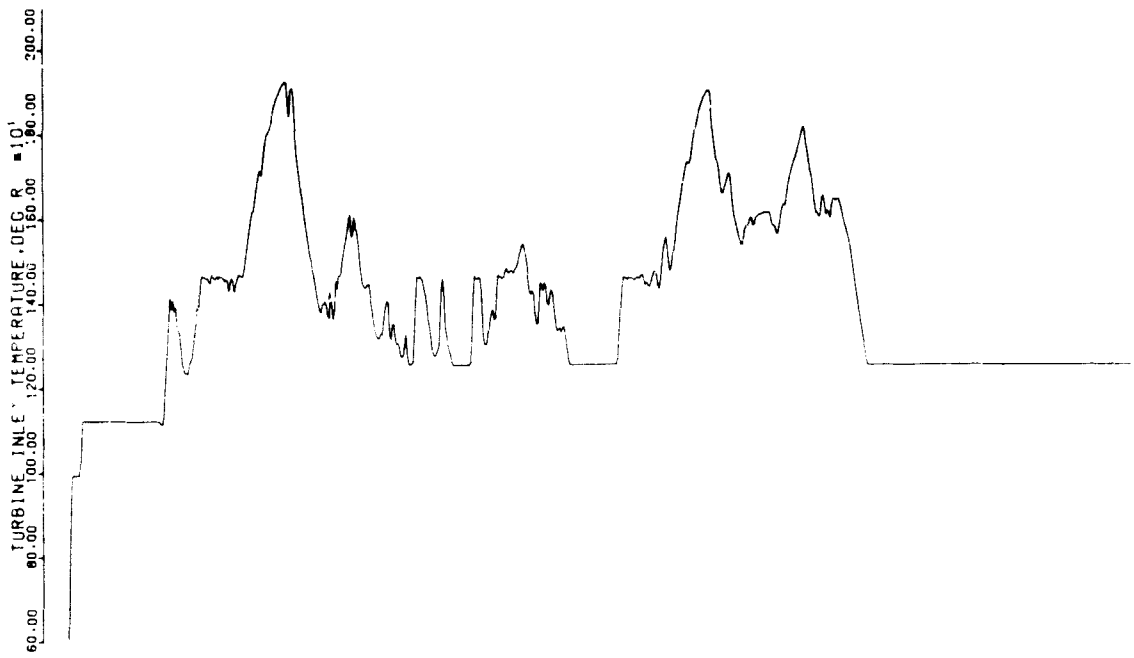


Figure 4-2. Temperatures for April 7, 1979 (100 lb of NaCl) A-17500

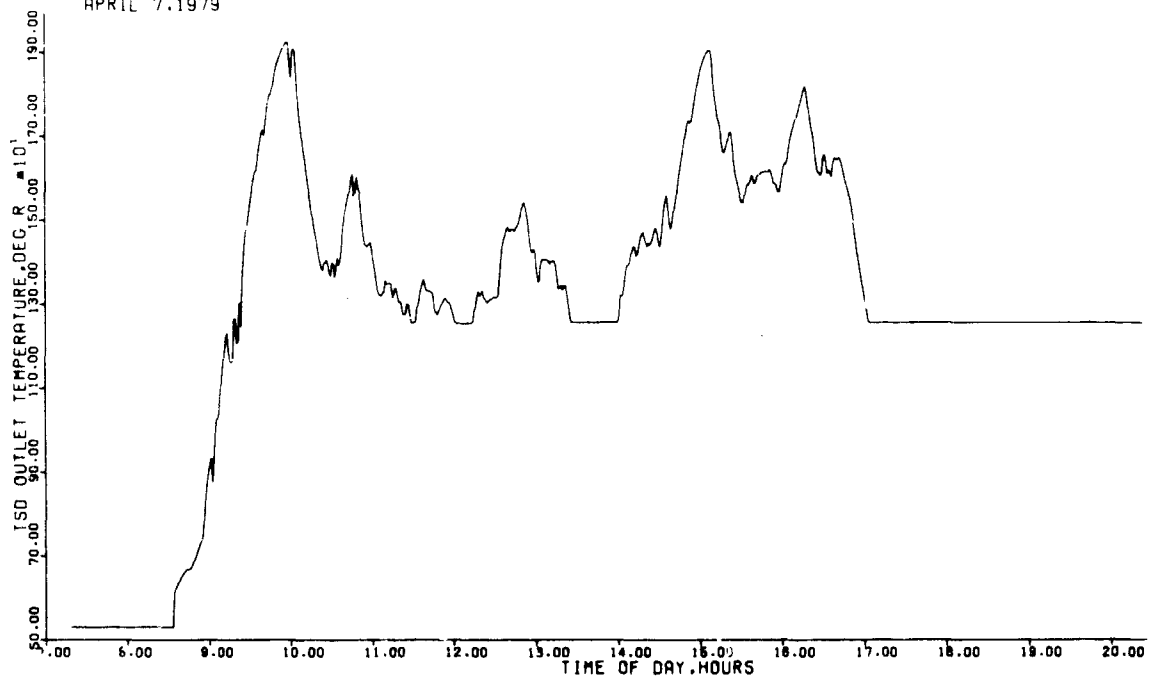






200 LB NACL (TC=1000 DEG F)

APRIL 7, 1979

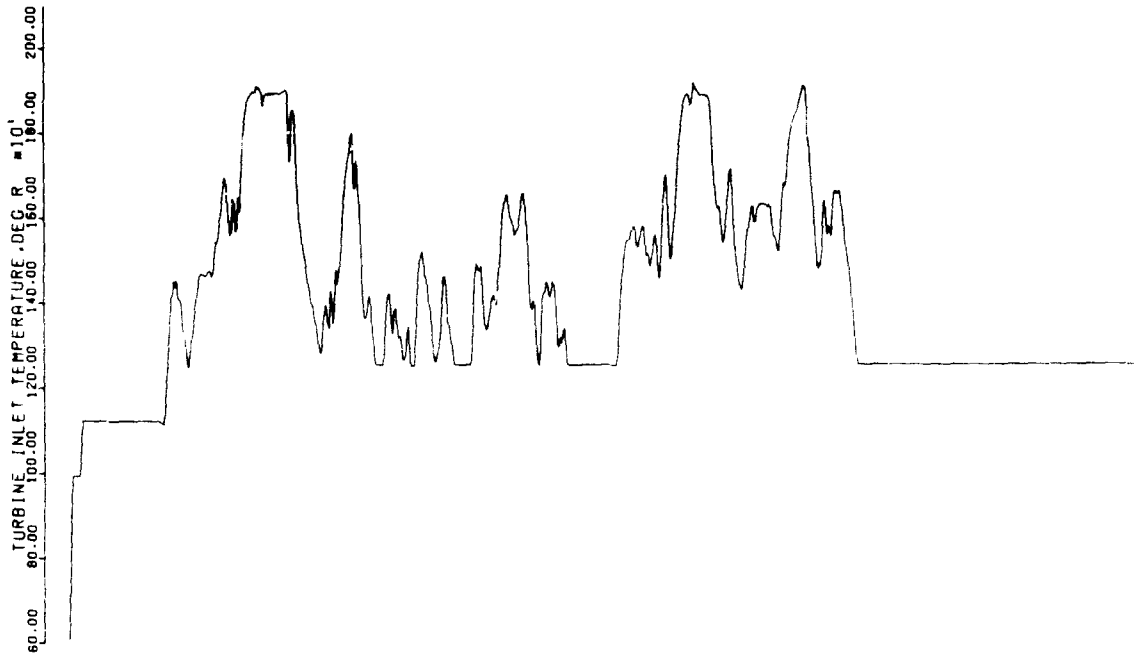


A-17501

Figure 4-3. Temperatures for April 7, 1979 (200 lb of NaCl)

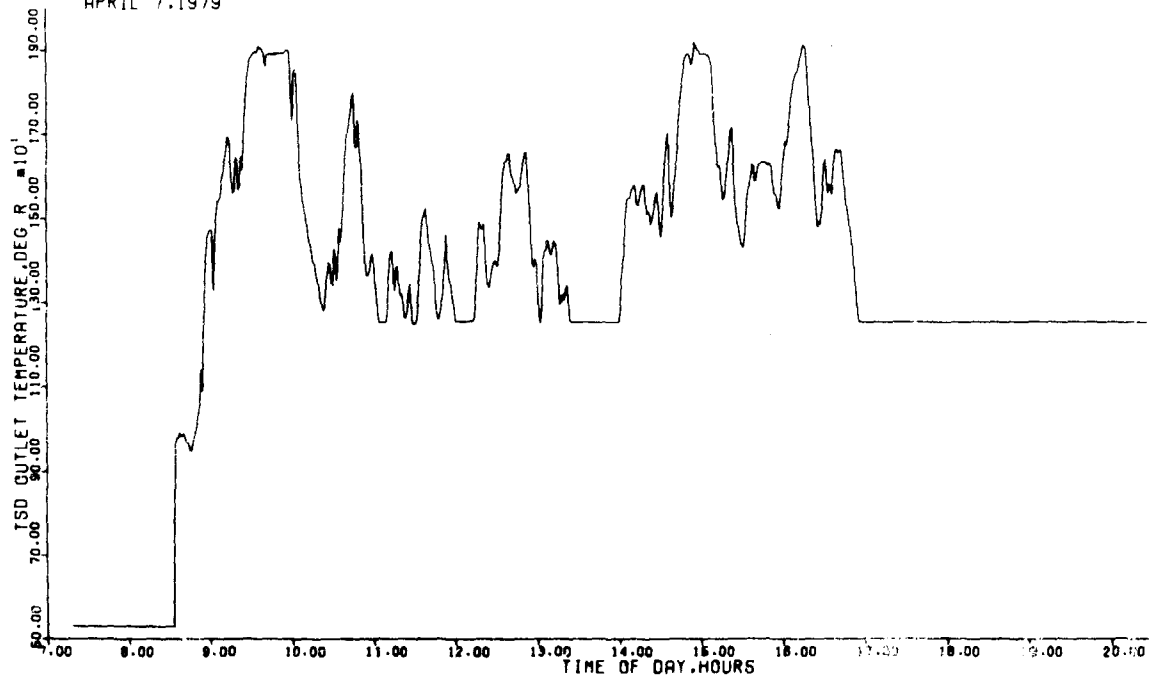


AIRESEARCH MANUFACTURING COMPANY



50 LB LI2CO3 (TC=1000 DEG F)

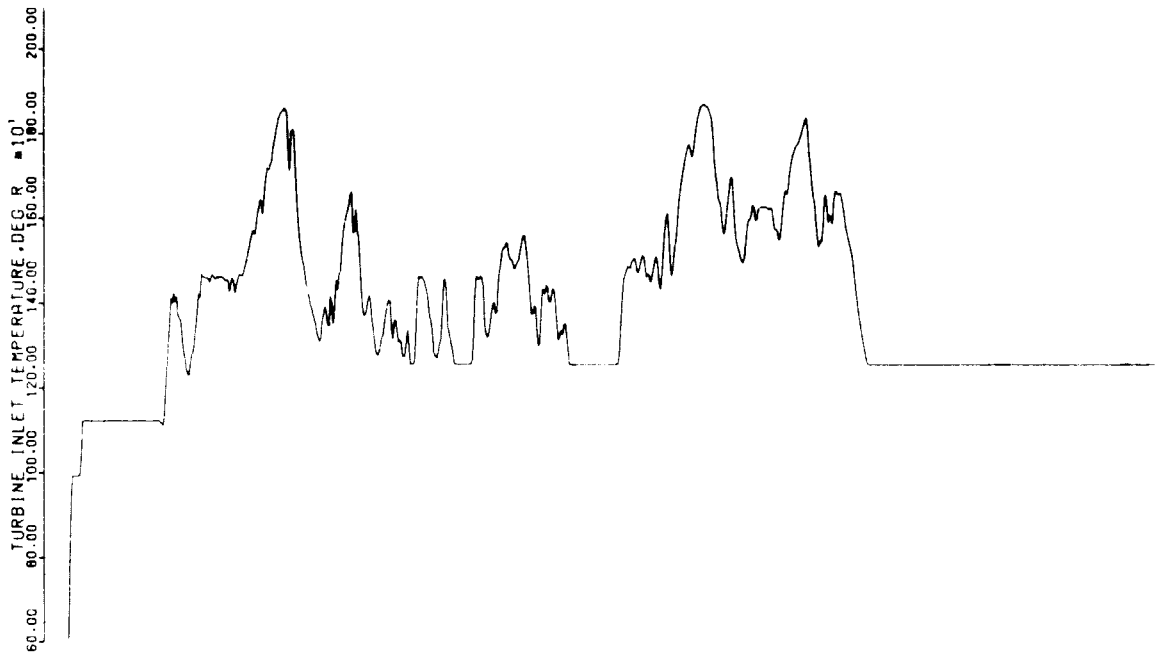
APRIL 7, 1979



A-17602

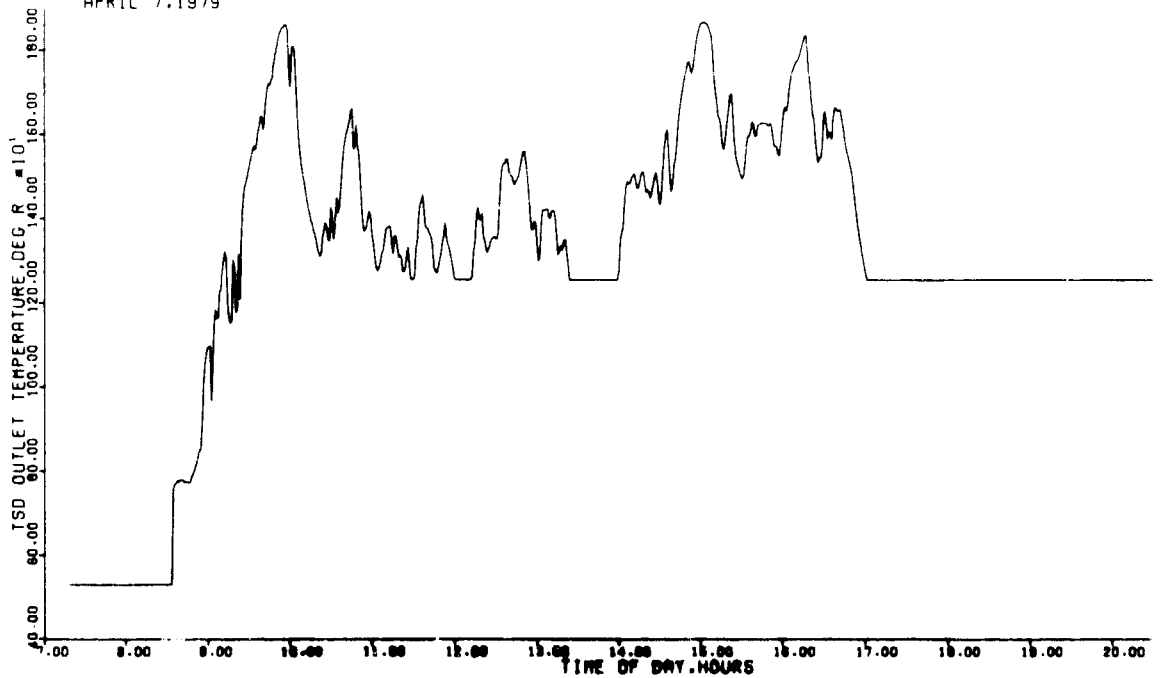
Figure 4-4. Temperatures for April 7, 1979 (50 lb of Li<sub>2</sub>CO<sub>3</sub>)





100 LB LI2CO3 (TC=1000 DEG F)

APRIL 7, 1979

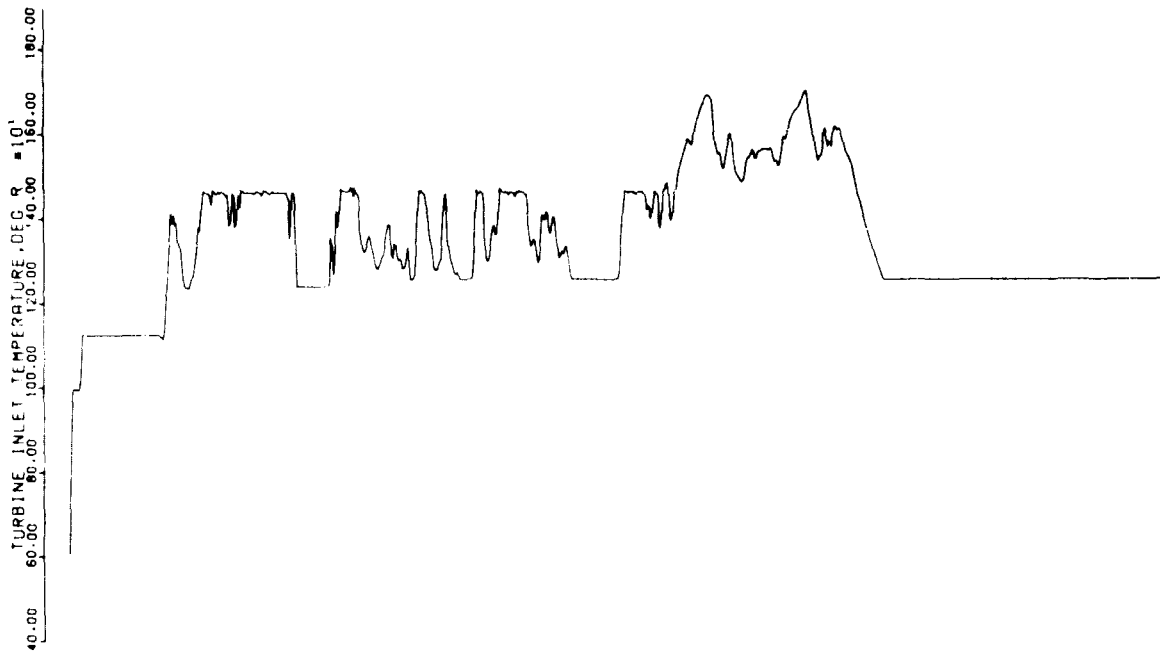


A-17803

Figure 4-5. Temperatures for April 7, 1979 (100 lb of  $Li_2CO_3$ )

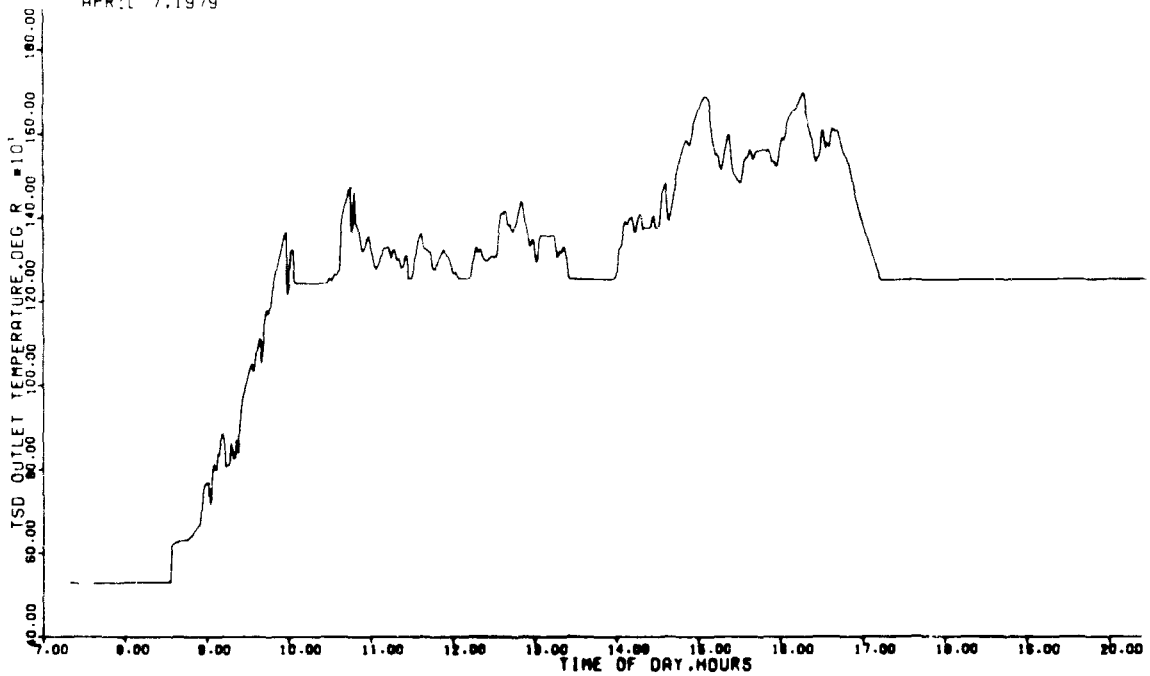


AIRESEARCH MANUFACTURING COMPANY



200 LB  $Li_2CO_3$  (TC=1000 DEG F)

APRIL 7, 1979



A-17804

Figure 4-6. Temperatures for April 7, 1979 (200 lb of  $Li_2CO_3$ )

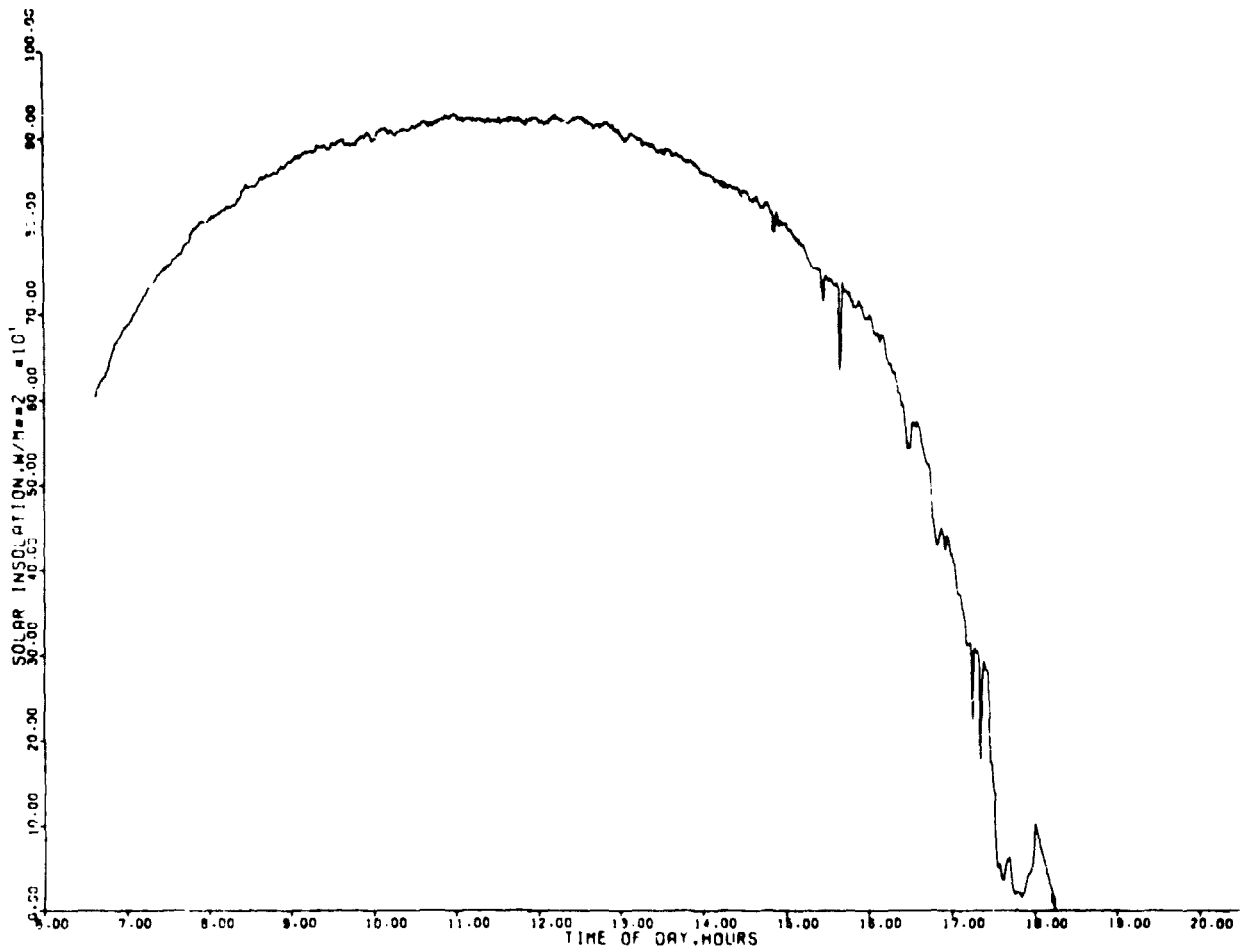


AIRESEARCH MANUFACTURING COMPANY

As the TSD heats up, the TIT is controlled at 1460°R. After the TSD reaches the TC (at about 9.5 hr), the TIT is allowed to increase. At this point, and for the rest of the day, the receiver and TSD are completely in series, i.e., full flow passes through the TSD. For the remainder of the day, the TSD can be observed to be heated and cooled as the insolation varies. Shutdown periods are observable as periods of constant TIT and TSD outlet temperature. It is significant to note that the TSD operates almost entirely in the sensible heat (solid PCM) regime during the day. There were a total of 8 engine shutdowns with the thermal storage; without thermal storage there were 14 shutdowns.

Comparison with the 200-lb  $\text{Li}_2\text{CO}_3$  case (Figure 4-6) clearly indicates the more rapid heat-up of the NaCl. As previously discussed, this is a result of the much lower heat capacity of NaCl. Heat-up time differences are also apparent for different weights of the same PCM.

Plots were also made for a clear day, April 20. The insolation is shown in Figure 4-7, and the output temperatures are shown in Figures 4-8 and 4-9 for 200 lb of NaCl and 200 lb of  $\text{Li}_2\text{CO}_3$ . For the clear day, the TSD operates primarily in the latent heat (two-phase PCM) regime.

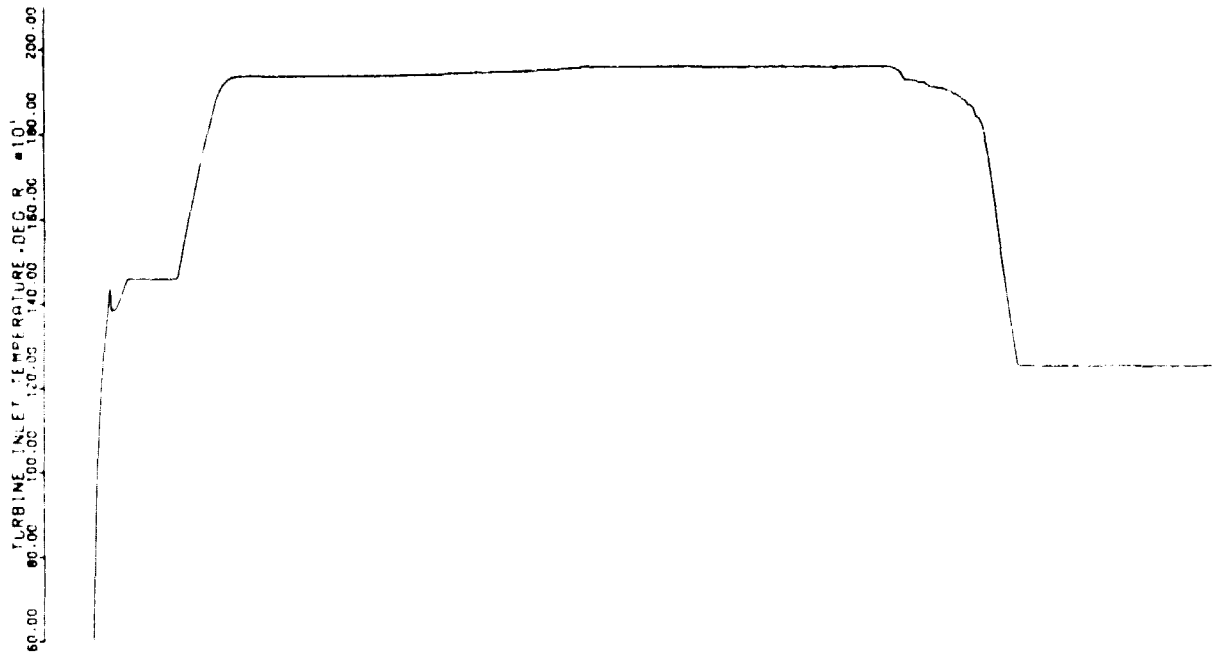


A-17505

Figure 4-7. Insolation Input for April 20, 1979

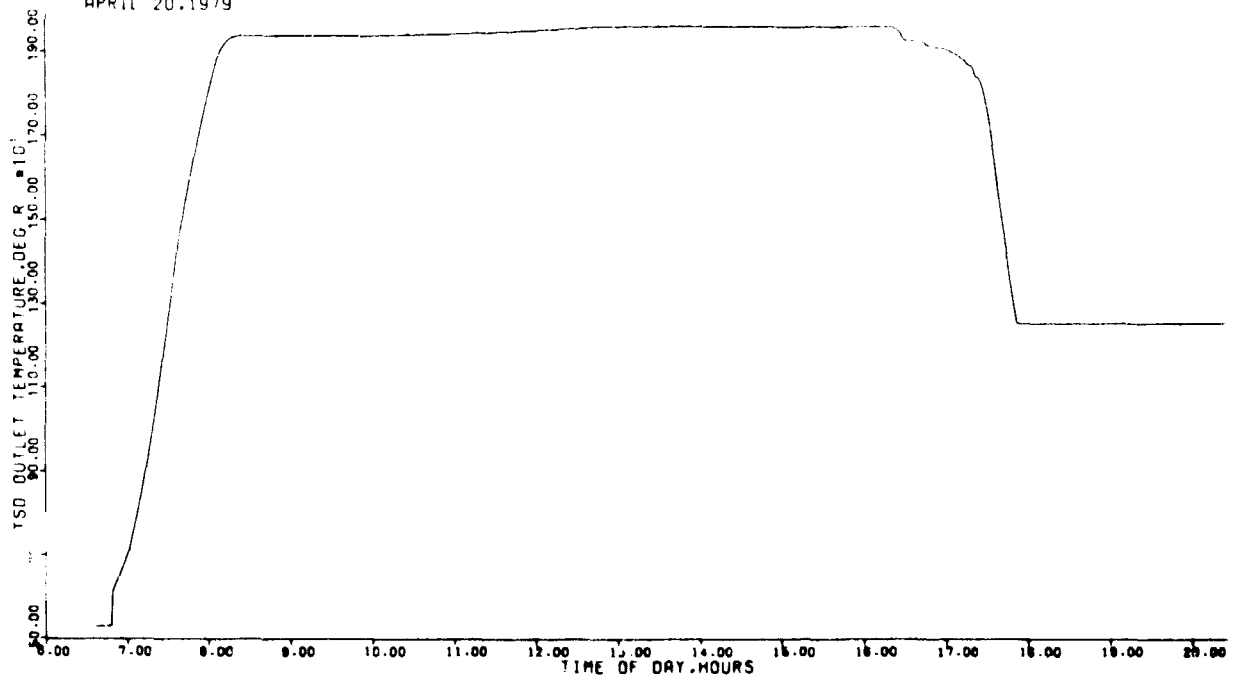


AIRESEARCH MANUFACTURING COMPANY



200 LB NAACL (TC=1000 DEG F)

APRIL 20, 1979

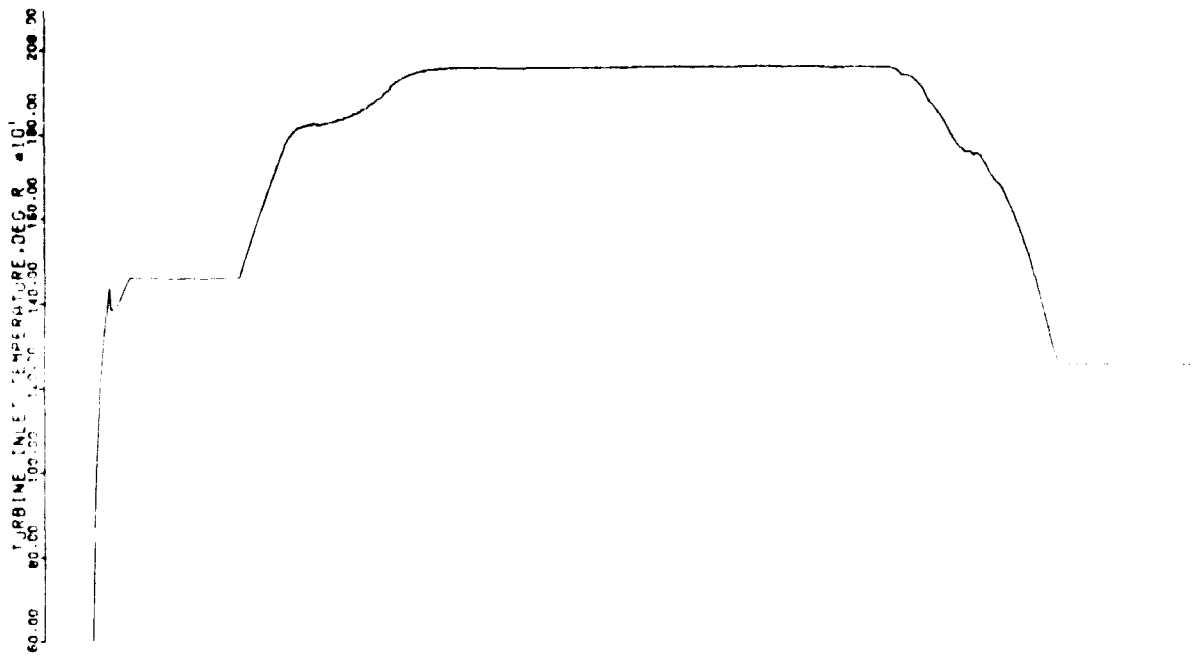


A-17508

Figure 4-8. Temperatures for April 20, 1979 (200 lb of NaCl)

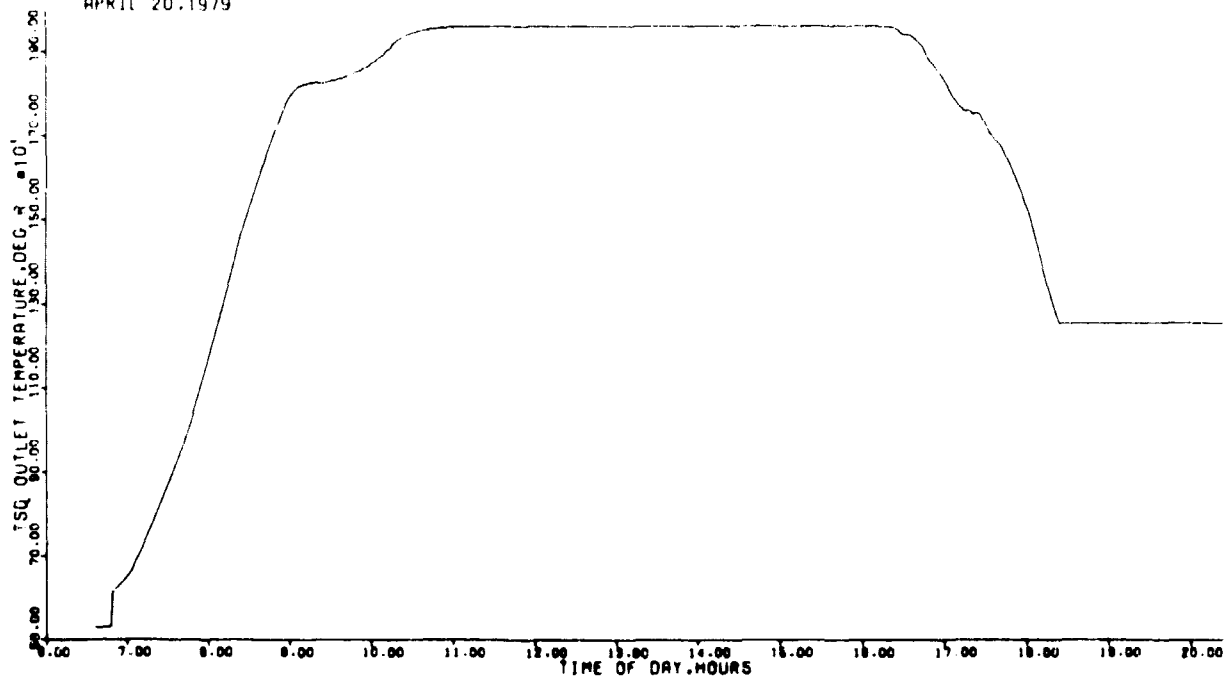


AIRESEARCH MANUFACTURING COMPANY



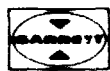
200 LB LI<sub>2</sub>CO<sub>3</sub> (TC=1000 DEG F)

APRIL 20, 1979



A-17887

Figure 4-9. Temperatures for April 20, 1979 (200 lb of Li<sub>2</sub>CO<sub>3</sub>)





## SECTION 5

### THERMAL STORAGE DEVICE CONCEPTUAL DESIGN

Although a thorough conceptual design study for the TSD is beyond the scope of the present effort, one conceptual design was prepared to elucidate the size and packaging requirements as well as to serve as a baseline for future cost estimation. The design is based on 200 lb of NaCl as the PCM; a TSD of this size yielded the minimum number of shutdowns (see Table 4-2).

The conceptual design is that of a shell and tube heat exchanger with two tube-side passes. The two-pass design is well suited to the orientation variations that would be encountered by a TSD mounted in the engine plane. With a single-pass design, if the tubes are in a near-horizontal orientation, some of the tubes may not be surrounded by PCM when the PCM is in the solid phase. This is because of the difference in density of the liquid and solid phases of the PCM (about 25 percent). Volume must be available to handle the entire PCM weight at its highest liquid temperature (1500°F). Thus, in the solid phase, substantial tube surface might not be covered with PCM. This could result in complete bypassing of some of the cycle air, resulting in a loss of heat exchanger effectiveness because there would be no heat transfer to these tubes. The two-pass design ensures that complete bypassing cannot occur regardless of heat exchanger orientation; all the tubes in one of the passes would always be covered.

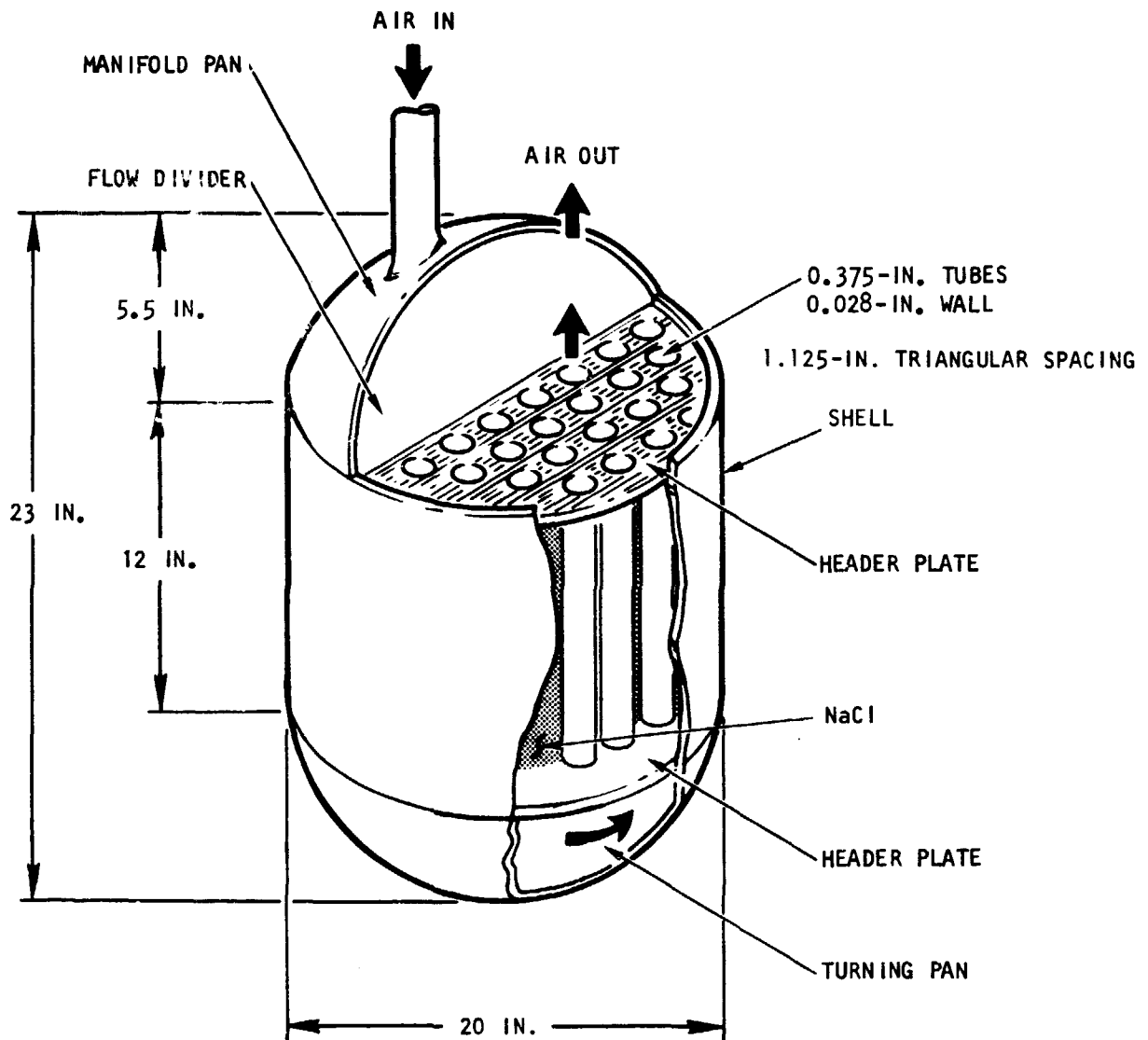
The conceptual design is shown in Figure 5-1. The tubes are brazed to the header plates to form a leak-tight and structurally sound unit. A flow divider is installed in the manifold to separate the inlet and outlet flow streams. A flow turning pan is provided at the opposite end to turn the flow for the second pass through the tubes. The device would be surrounded by 4 to 5 in. of high-temperature insulation.

The unit is sized to yield sufficient heat transfer area when the PCM is solid. Additional volume is available for PCM expansion during melting. Thus, about 25 percent of the tube surface area may be uncovered when the PCM is solid.

To maintain the TSD pressure drop at 2 percent of the inlet pressure at the design flow (0.6 lb/sec), it was necessary to use a minimum tube diameter of 0.375 in. The 0.25-in. tube diameter used for the computer runs (see Appendix A) results in a pancake shape for the two-pass configuration. The tube spacing was selected to maintain the value of the resistive path length used in the computer runs (0.375 in.). The resulting design does not, however, exactly match the cycle fluid thermal conductance used previously. Thus, more precise performance prediction awaits using the appropriate parameters of the conceptual design in the computer runs.

As shown in Figure 5-1, the overall length is about 23 in. (including manifold and pan) and the diameter is 20 in. There are 268 tubes. The tubes and shell are expected to be made of type 321 SS. This material has performed well in compatibility tests conducted by JPL with molten NaCl. The tube weight is about 30 lb. The shell (including ends) weighs 40 to 50 lb, depending on the wall thickness used. The PCM weight is about 220 lb, including about 10 percent excess.





S-34592-A

Figure 5-1. Conceptual Design of Thermal Storage Device (TSD)

## SECTION 6

### ECONOMIC ANALYSIS

Incorporation of buffer thermal storage in the solar Brayton engine has been shown to decrease the number of engine shutdowns and, hence, increase engine life. This additional engine life is, of course, offset by the increased initial cost attributable to the TSD and associated hardware. The economic analysis presents a tradeoff of these costs and savings in an effort to determine the economic viability of thermal storage.

In general, achieved engine life is a function of the number of start-stop cycles and the total number of operating hours. This makes it especially difficult to predict engine life for new applications, given the scant data available for engines of this type. It has thus been decided to treat engine life parametrically, rather than make a prediction, in this economic study. To simplify the investigation, engine life has been assumed to be relatively insensitive to operating hours; it will be treated only as function of the number of start-stop cycles.

Engine cost, on the other hand, has been investigated for this application. By scaling cost information for a 10-kw(e) subatmospheric engine, Fortgang and Mayers of JPL have determined required selling prices for a 20-kw(e) solar Brayton engine for various annual production volumes.\* This is essentially equivalent to the Mod "O" engine used for the present study. Fortgang and Mayers determined a selling price of \$5328 for the engine at a production rate of 1000 units per year (the lowest production rate studied). This value is used in the present study. It is assumed that the entire engine replacement cost of \$5328 must be met at engine failure. In actuality, some engine repair may be possible for certain types of failures; this uncertain situation is not considered.

The life of the TSD is not likely to be cycle-dependent. The large thermal inertia of the device results in only moderate transient effects. Long-term creep and interaction with the molten PCM will make the TSD life largely a function of service life. The TSD replacement cost, which is treated parametrically, is assumed to be completely met at TSD failure.

In addition to the TSD itself, other costs are associated with the thermal storage system. The major item is the high-temperature three-way valve, but there are additional piping, control, and support costs. These are approximated by a fixed cost of \$10,000. This is a one-time investment and does not have to be repeated over the 30-yr design life of the power plant.

There is also an energy production penalty associated with using thermal storage (see Table 4-2). This will be assigned a value of 80 mills/kwhr.

\*H.R. Fortgang and H.F. Mayers, "Cost and Price Estimate of Brayton and Stirling Engines in Selected Production Volumes," JPL Publication 80-42 May 1980.

The results of the parametric calculations are presented in Figure 6-1, which shows the break-even TSD cost as a function of TSD and engine life. The calculations were performed in such a manner that they could be readily repeated using other cost assumptions and information. The TSD with 200 lb of NaCl was used in the calculations. From Table 4-2 it can be seen that the number of yearly cycles for the engine is 1084 with thermal storage and 1810 without thermal storage. Since the engine cost is \$5328, the cost per year is given by:

$$\$5328/(N/1084) \text{ with thermal storage}$$

and

$$\$5328/(N/1810) \text{ without thermal storage}$$

where N is the cycle life of the engine

The energy differential is  $44676 - 40723 = 3953$  kwhr, equivalent to \$316.24/yr if the cost is 80 mills/kwhr. The fixed cost per year for TES is  $10,000/30 = \$333.33/\text{yr}$ .

The savings per year afforded by the thermal storage is given by:

$$5328/(N/1810) - 5328/(N/1084) - 316.24 - 333.33$$

The break-even TSD cost is the savings per year multiplied by the life of the TSD.

Examination of Figure 6-1 indicates that the economic viability of buffer TES is largely a function of achievable engine life. At low predicted life, TES is economically attractive; at greater engine life, TES is less attractive. Indeed, if the engine life is greater than about 6000 cycles, the TSD is not profitable at any cost, because the engine cost savings are balanced by the fixed cost and energy differential.

It should be pointed out that certain costs associated with replacing an engine have not been considered. These include the labor costs and the value of the energy lost during power plant downtime. Inclusion of these costs would tend to improve the economic position of TES. The same general conclusion still applies however--attainment of high engine reliabilities precludes the advantage of buffer thermal energy storage. For less reliable engines, thermal storage may be a cost-saving approach.



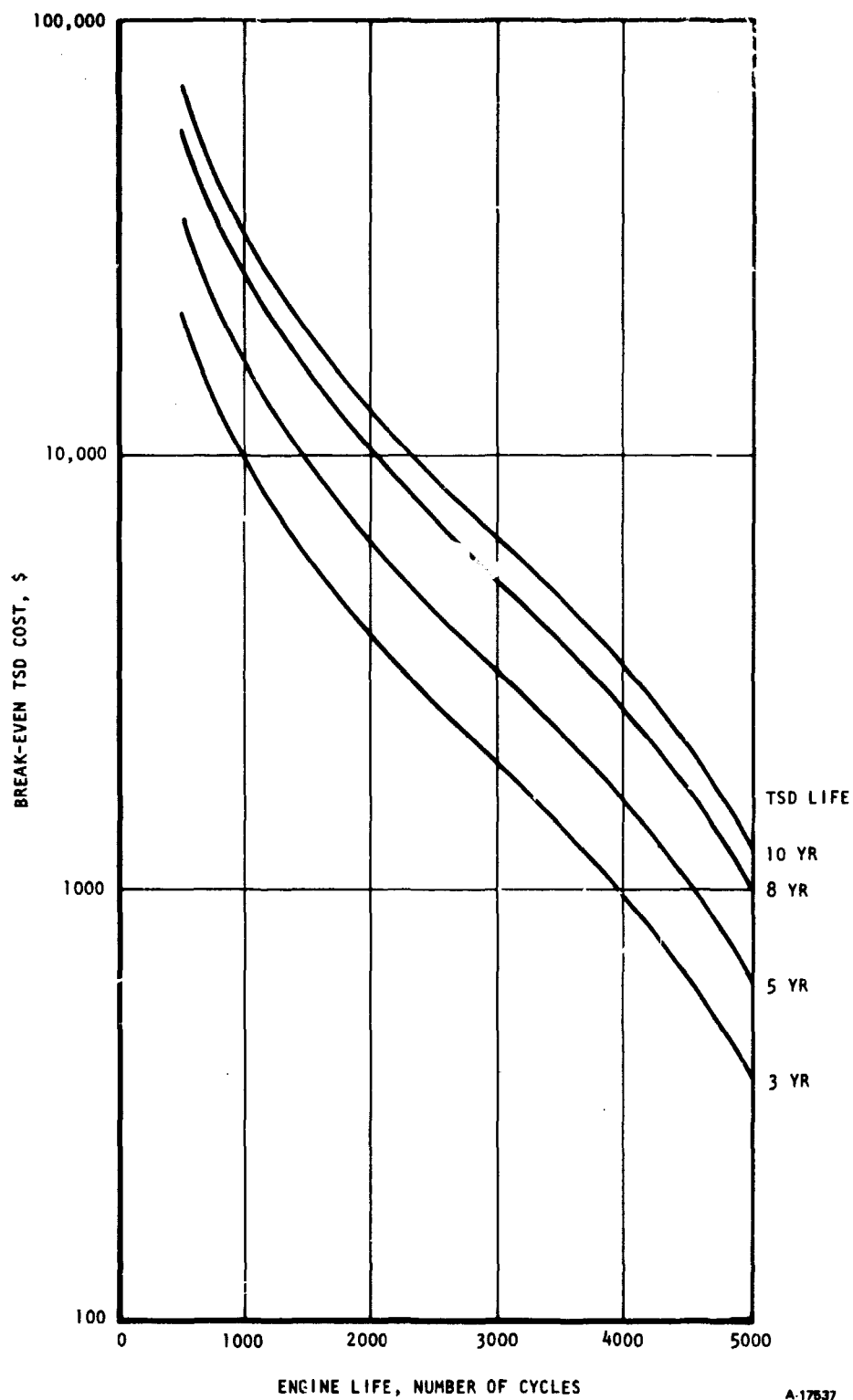


Figure 6-1. Break-Even Cost for a 2C0-1b-NaCl TSD



## SECTION 7

### CONCLUSIONS AND RECOMMENDATIONS

#### CONCLUSIONS

The following itemized remarks summarize the results and conclusions of the study:

- (a) A complete transient/steady-state Brayton-cycle performance computer program was written. The program models the recuperator, receiver, and TSD as finite-element thermal masses; actual operating or predicted performance data are used for all components, including the rotating equipment.
- (b) Thermal storage can afford a significant decrease in the number of engine shutdowns as compared to operating without thermal storage. This results in an increase in engine life.
- (c) The number of shutdowns does not continuously decrease as the PCM weight increases. In fact, for a given storage material, there appears to be an optimum weight for minimizing the number of shutdowns.
- (d) An economic parametric study indicated that the economic viability of buffer TES is largely a function of achievable engine life. At low predicted life, thermal storage is economically attractive; for highly reliable, long-lived engines, thermal storage is not economical.

#### RECOMMENDATIONS

The following suggestions for future work are offered:

- (a) Since the computer program is fully operational, additional thermal storage conditions and/or simulated years could be run to further investigate trends and optimize the storage material and capacity.
- (b) Further investigation of the viability of the selected engine control scheme and a consideration of other control schemes should be undertaken.
- (c) Development of cost models for the engine, TSD, and high-temperature valve based on similar assumptions is necessary for further economic analysis.
- (d) Accurate engine life-cycle prediction, along with an accurate estimate of TSD life, is also necessary for improved economic analysis.



APPENDIX A

SOLAR BRAYTON COMPUTER PROGRAM

## APPENDIX A

### SOLAR BRAYTON COMPUTER PROGRAM

#### GENERAL METHOD OF SOLUTION

A transient calculation implies the investigation of the time dependence of the variables that describe the state of the system. Two types of variables can be distinguished: those with a long (compared to some arbitrary standard) time-constant and those with a short time-constant. Choice of the standard will depend on the specific performance question being asked. This distinction is important because it affects how the variables are treated in the model. The variables with a long time-constant are treated in a true transient fashion; the others are treated at any given time as being in equilibrium with the prevailing values of the transient variables and the boundary conditions (which also may be time-dependent).

For example, a sudden change in the controlled turbomachinery speed would result in almost simultaneous changes in the flows and pressures around the circuit. But, because of the thermal inertia of the recuperator, its internal metal temperatures would not immediately show a large change. The temperatures of massive solid elements, therefore, are treated in a proper transient fashion using transient equations to calculate the temperature changes during each time step due to the temperature gradients around and the conductive, convective, and/or radiative couplings to each massive node. The temperature changes are proportional to the time step. Furthermore, the assumption is made that the time step has been chosen small enough that the gradients and couplings remain unchanged over the interval. On the other hand, the flows and pressures (and the turbomachinery speed when this is not controlled to a given value) are found from steady-state relations. This usually involves a set of nonlinear simultaneous equations, the solution of which determines the flows, temperatures, etc., that would be in equilibrium with the boundary conditions and the current temperatures of all the massive elements at some instant of time. Because the working fluid capacity rates (mass flow multiplied by specific heat) are small, the fluid temperatures are also found from steady-state relationships.

The transient calculation proceeds, then, with the performance of two calculations at each time step. These are:

- (a) From the prevailing boundary conditions and solid temperatures (either as input for the first time step or as previously calculated for subsequent steps), the system equations are solved for flows, pressures, rotating speed, and fluid temperatures.
- (b) The transient calculation is performed to find the new solid temperatures, using the flows and fluid temperatures just determined.

The system equations in the first calculation are expressions of pressure equalities, energy balances, temperature identities, etc., that must be satisfied. They are solved using an N-dimensional Newton technique. This is an iterative method that involves a series of successive linearizations. The general development and solution of these equations is discussed below, followed by a description of the methods used in the second calculation to find the transient solid node temperatures for each massive component in the system.



Development of the System Equations

Figure A-1 shows the system modeled by SOLARBAYTON with the station and flow numbering indicated. At any time there will be known values of all the boundary conditions and the slowly responding temperatures of the solid elements of the massive components (recuperator, receiver, and thermal storage device). The values of the quickly responding variables (pressures, flows, fluid temperatures, etc.) that at that time are in equilibrium with these boundary conditions and solid temperatures are found by solving a set of system equations as described below.

Let  $\{x^{(j)}\}$  represent the set of  $N$  independent variables (yet to be specified) and let  $f^{(i)}(\{x^{(j)}\}) = 0$  be one of the  $N$  equations (generally non-linear) that the system of Figure A-1 must satisfy. Three types of  $f^{(i)}$  appear in SOLARBAYTON. The first type results from the physics of the situation, an example being the pressure closure condition

$$f^{(1)}(\{x^{(j)}\}) = \sum_{\substack{\text{over all} \\ \text{components in loop}}} \Delta P_k = 0 \quad (1)$$

where  $\Delta P_k$  is the pressure rise or drop in the  $k$ th component. A second type of  $f^{(i)}$  results from specific system performance requirements. For example, demanding a specific turbine inlet temperature ( $T_8$ ) is stated mathematically as

$$f^{(2)}(\{x^{(j)}\}) = T_8 - TR = 0 \quad (2)$$

where  $TR$  is the desired temperature.

The third type of  $f^{(i)}$ , introduced as a mathematical convenience, is discussed shortly. First, it is necessary to discuss the  $\{x^{(j)}\}$ . The choice of the  $N$  variables to be the  $\{x^{(j)}\}$  is influenced by the specific performance question being answered, but it is not always unique. Convenience and programmer preferences play a role. If  $f^{(1)}$  and  $f^{(2)}$ , above, were applied to the system of Figure A-1, a convenient choice would be the total flow,  $W(1)$ , and the turbomachinery speed,  $Nt$ . The problem reduces to finding values of  $Nt$  and  $W(1)$  so that, starting at the compressor inlet and calculating the pressure drops and temperatures around the circuit,  $T_8$  is the required value and the sum of the  $\Delta P$ 's is indeed zero. From an initial estimate of the system variables,  $\{x_1^{(j)}\}$ , which generally lead to  $f^{(i)}(\{x_1^{(j)}\}) \neq 0$ , better estimates are developed until on the  $n$ th iteration the equations satisfy  $f^{(i)}(\{x_n^{(j)}\}) < \epsilon$  where  $\epsilon$  is some convergence criterion.

There are many other variables in the system besides  $W(1)$  and  $Nt$ : temperatures, pressures, and pressure ratios, for example. But these can all be straightforwardly evaluated once iterative values of  $W(1)$  and  $Nt$  are provided. Thus, these other variables can be mathematically eliminated to reduce the problem to one of only a few equations in a few unknowns from one of many equations in many unknowns.

A third type of  $f^{(i)}$  can result from various mathematical procedures. For example, component performance information may specify via equations, tables, or maps some quantity  $y=y(z)$ , where  $y$  may be either one of the  $\{x^{(j)}\}$  or one of the other variables known once the  $\{x^{(j)}\}$  are specified. The evaluation of  $z$



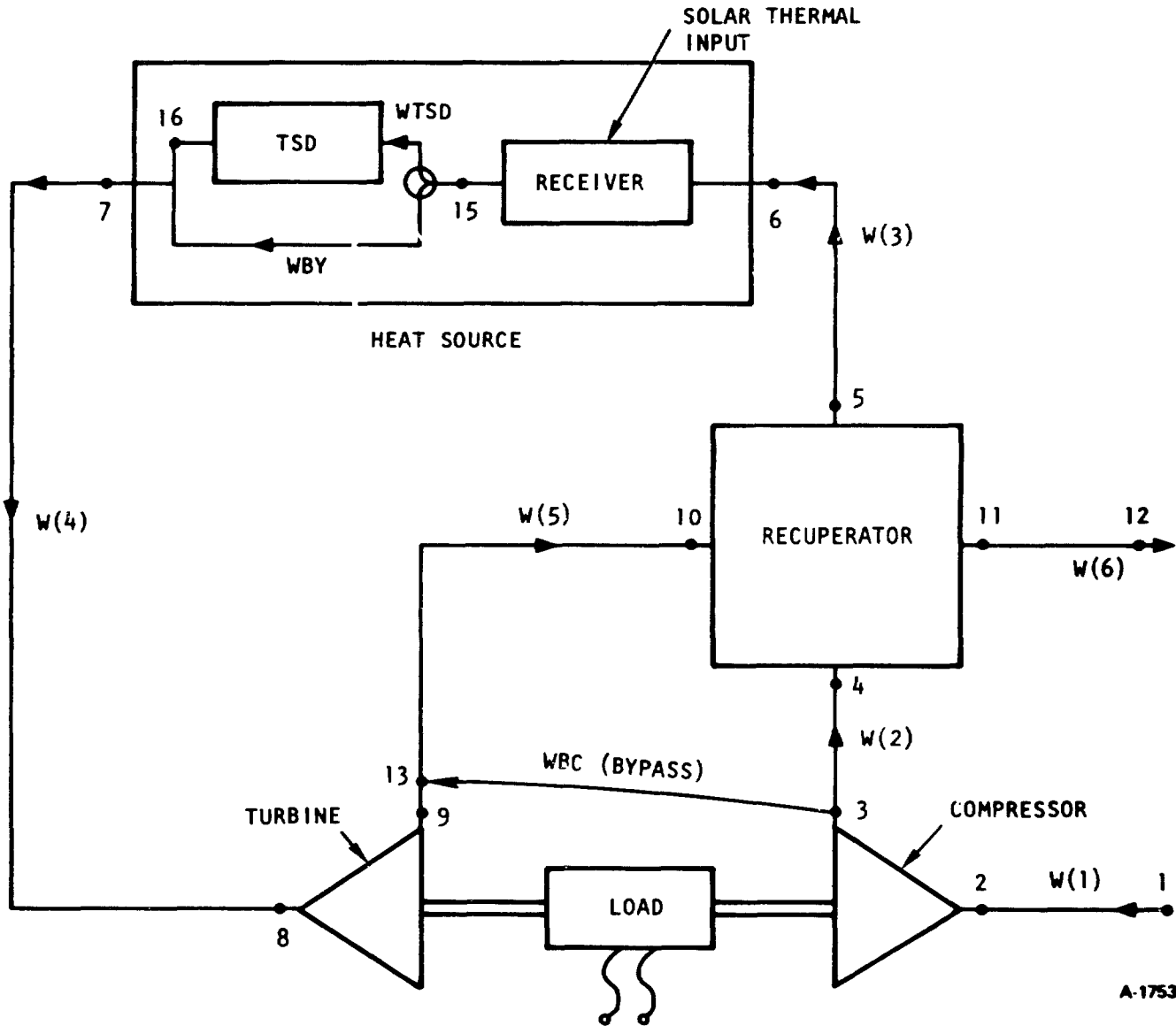


Figure A-1. Computer Model Schematic

from  $y$  and  $y=y(z)$  may lead to computational difficulties for a number of reasons. Ambiguity may result if  $y=y(z)$  is not a monotonic function of  $z$ . Or, if  $y$  is bounded, a problem will result if an iterative value of  $y$  exceeds, even by the slightest amount, the range of  $y$ . The problem is readily solved, however, by adding  $z$  to the  $\{x^{(j)}\}$ . When the circuit calculation arrives at the component in question with the iterative value  $y_n$ , instead of finding  $z(y_n)$ , the iterative value  $z_n$  (one of the  $\{x^{(j)}\}$ ) is used to continue around the circuit. In addition,  $y(z_n)$  is calculated and

$$f(3) = y_n - y(z_n) = 0 \quad (3)$$

is added to the set of system equations that must be solved to determine the  $\{x^{(j)}\}$ . This technique is used by SOLARBRAYTON to avoid some reading difficulties with the turbomachinery performance maps.

### Solution of System Equations

Sets of simultaneous, nonlinear equations can be solved efficiently by the method of Newton (also called the Newton-Raphson method). This is an iterative technique that involves a series of successive linearizations. Consider, for simplicity, one nonlinear equation in one unknown,

$$f(x) = 0 \quad (4)$$

If  $x_n$  is the  $n$ th trial solution, then the closure error is defined by

$$e(x_n) = f(x_n) \quad (5)$$

and the problem reduces to finding  $x_n$  so that  $e(x_n)$  is less than some given convergence limit. To find an iteration formula for  $x_{n+1}$  in terms of  $x_n$ , a Taylor expansion of  $e(x_n)$  about  $x_n$  is made, keeping only the linear terms. This gives

$$e(x_{n+1}) = e(x_n) + \left. \frac{de}{dx} \right|_{x=x_n} (x_{n+1} - x_n) \quad (6)$$

Setting  $e(x_{n+1})$  to the desired value of zero and solving for  $x_{n+1}$  gives the Newton-method iteration formula:

$$x_{n+1} = x_n - \left[ \left. \frac{de}{dx} \right|_{x_n} \right]^{-1} e(x_n) \quad (7)$$

Replacing the inverse derivative factor by a constant (usually less than or equal to 1) results in the simpler but less rapidly converging iteration formula of the method of successive substitutions. An intermediate approach is to use the iteration formula defined by

$$x_{n+1} = x_n - \left[ \left. \frac{de}{dx} \right|_{x_1} \right]^{-1} e(x_n) \quad (8)$$



where  $x_1$  is the initial estimate of  $x$ . The use of Equation (8) instead of the Newton formula given by Equation (7) would result in more steps to reach convergence, but each step after the first would involve fewer computations.

The AiResearch method of solving nonlinear equations involves the use of both of the iteration formulae of Equations (7) and (8). Rather than evaluate new derivatives at each iteration, the old derivatives are used as long as they give satisfactory reductions of the closure errors. When the rate of convergence is not satisfactory, then new derivatives are evaluated to speed the convergence.

The extension of Equation (7) to a set of  $N$  equations in  $N$  unknowns, each of the form

$$f^{(i)}(\{x^{(j)}\}) = 0 \quad (9)$$

is a straightforward extension of the method outlined above and is discussed in numerical analysis texts and references.\* If  $X_n$  is the vector whose components  $x_n^{(j)}$  are the  $n$ th iterative values of the individual independent variables, and if  $E_n$  is the vector whose components  $e^{(i)}(\{x_n^{(j)}\})$  are the individual closure errors each of which is a function of the  $n$ th iterative values of the entire set of independent variables, then the multidimensional generalization of Equation (7) is simply

$$X_{n+1} = X_n - J_n^{-1} E_n \quad (10)$$

where  $J_n^{-1}$  is the inverse of the  $N \times N$  Jacobian matrix with elements

$$J_n(i,j) = \left. \frac{\partial e^{(i)}}{\partial x^{(j)}} \right|_{\{x^{(j)}\} = \{x_n^{(j)}\}} \quad (11)$$

Clearly, Equation (10) reduces to Equation (7) for  $N = 1$ .

A similar multidimensional generalization can be written for Equation (8). The evaluation of the derivatives (usually by numerical methods) and the inverting of the matrix can involve considerable amounts of computation time. Therefore, the program that implements the solution of the set of simultaneous nonlinear equations must be judicious in choosing when to evaluate a new Jacobian matrix and to find its inverse and when to continue to use the one from a previous iteration.

\*For example: E. K. Blum, Numerical Analysis and Computation: Theory and Practice, Addison-Wesley, 1972; A. S. Householder, Principles of Numerical Analysis, McGraw-Hill, 1953.



When the relationships given by Equation (9) represent relations among physical quantities as they do in this study, it is usually best to write them in a nondimensional form. This allows a magnitude of the closure error vector to be evaluated by taking the square root of the sum of the squares of the individual, nondimensional, closure errors. It is this magnitude that is usually tested against a specified convergence criterion.

### Temperatures of Solid Elements

The solid mass of the solar Brayton system is mostly concentrated in the heat transfer equipment--the recuperator, the receiver, and the thermal storage device. These items therefore are analyzed by finite element models to properly evaluate the effects of their finite thermal capacity on system performance.

The recuperator finite-element model is illustrated in Figure A-2. In this model the multipassage nature of the recuperator is represented by a single passage for each stream, separated by the total mass of the heat exchanger. The solid core and the two fluid passages are divided into  $N$  elements (or nodes) in the longitudinal (i.e., flow) direction; the transverse direction is divided into only three elements, one solid and two fluid. At any instant of time, each solid element is characterized by one temperature, considered to be uniform over the element. For each fluid element in contact with a solid node, temperature varies exponentially from inlet to outlet. This steady-state temperature distribution for a fluid flowing past a uniform temperature solid is derived in standard heat transfer texts. Thus, for the fluid passages there are  $N + 1$  nodal temperatures associated with the  $N$  fluid elements, as shown in Figure A-2.

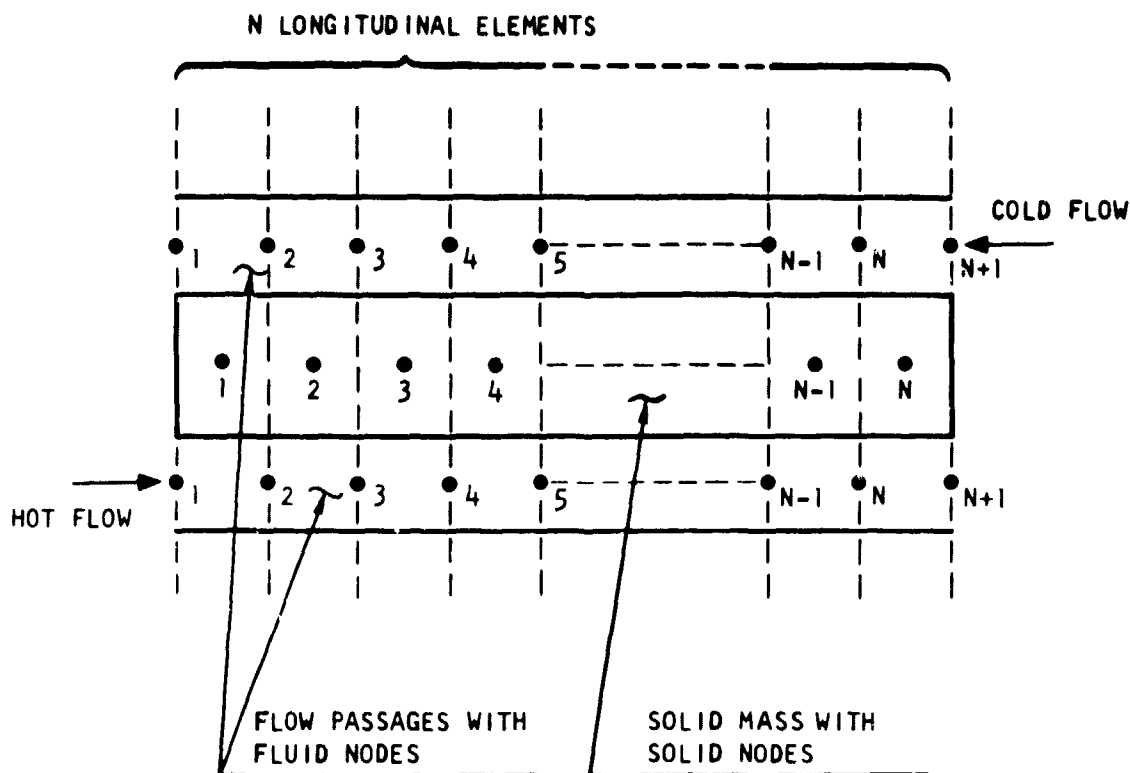
For the  $i$ th solid node in the heat exchanger, the thermodynamic problem is to find the temperature of the node at a time  $t' = t + \Delta t$ , given the physical and geometrical properties of the element, the temperature,  $T_i^{(s)}$ , of the element, and the temperatures,  $T_j$ , of all the nearest-neighbor solid and fluid nodes, all at time  $t$ . That is, calculate

$$T_i^{(s)}(t') = f(\{T_j(t)\}; \text{physical, geometrical properties}; \Delta t) \quad (12)$$

It should be noted that the right-hand side of Equation (12) is written entirely in terms of quantities known at the time  $t$ . The computation is therefore quite straightforward and much of the programming effort reduces to careful bookkeeping to step through all the solid nodes of the system.

An explicit expression for Equation (12) can be obtained by calculating the temperature change in the  $i$ th solid element during the time interval  $\Delta t$  due to all the surrounding temperature gradients.\* The average temperature difference from a fluid passage to a solid element is given by the log mean temperature difference due to the exponential temperature profile of the fluid. This leads to the following expression for  $T_i^{(s)}(t')$ :

\*For example: G.M. Dusinberre, Heat Transfer by Finite Differences, International Textbook Co., 1961.



S44448 A

Figure A-2. Recuperator Model with Node Identification

$$T_i^{(s)}(t') = T_i^{(s)}(t) + \frac{\Delta t}{C_i} \left\{ \sum_j K_{ij} [T_j^{(s)}(t) - T_i^{(s)}(t)] + \sum_k H_{ik} \Delta T_{LM, ik} \right\} \quad (13)$$

where

$C_i$  = thermal capacity of the  $i$ th element (mass of element times specific heat)

$K_{ij}$  = conductive coupling strength (thermal conductivity times cross sectional area divided by average separation) connecting the  $i$ - and  $j$ th solid nodes

$H_{ik}$  = convective coupling strength or thermal conductance (heat transfer coefficient times heat transfer area times overall fin efficiency) connecting the  $i$ th solid element with the  $k$ th nearest-neighbor fluid element ( $k$  is 1 for the hot fluid and 2 for the cold fluid)

The log mean temperature difference is defined as:

$$\Delta T_{LM, ik} = \frac{T_{ik}^{(f)} - T_{i+1,k}^{(f)}}{\ln \left[ \frac{T_{ik}^{(f)} - T_i^{(s)}}{T_{i+1,k}^{(f)} - T_i^{(s)}} \right]} \quad (14)$$

The subscripts in the above definitions assume that the fluid temperatures are numbered relative to the solid node temperature as indicated in Figure A-2. The superscripts represent either fluid (f) or solid (s) temperatures.

Because Equation (13) uses temperature differences throughout the interval  $\Delta t$  evaluated at the beginning of the interval, its accuracy depends on the size of  $\Delta t$ . The maximum allowed value of  $\Delta t$  is inversely related to the response rate of the element to the surrounding temperature gradients. Intuitively, this is proportional to the  $K_{ij}$  and  $H_{ik}$  and inversely proportional to  $C_i$ . By replacing  $\Delta T_{LM}$  with its geometric average, Equation (13) can be cast into a form (see Dusinberre, loc. cit.) that clearly shows that  $\Delta t$  must be constrained by the relation

$$\Delta t < \frac{C_i}{\sum K_{ij} + \sum H_{ik}} \quad (15)$$

The model for the receiver is similar to that of the recuperator, but there are two major differences. First of all, there is only one fluid passage, so that the sums over  $k$  in Equations (13) and (15) disappear. Secondly, the solar heat input that is carried away by the cooling fluid is introduced directly to the solid nodes. Mathematically, this is accomplished by adding a term  $q_i$  inside the curly bracket in Equation (13), where  $\sum q_i$  equals the net absorbed solar flux. Future solid temperatures for these components are then given by:

$$T_i^{(s)}(t') = T_i^{(s)}(t) + \frac{\Delta t}{C_i} \left\{ \sum_j K_{ij} \left[ T_j^{(s)}(t) - T_i^{(s)}(t) \right] + H_i \Delta T_{LM, i} + q_i \right\} \quad (16)$$

The thermal storage device can be considered to be a heat exchanger with a single fluid (air) in contact with the massive PCM (which is modeled to include the heat exchanger walls). As such, the TSD can be modeled in a manner similar to that of the receiver. Depending on the nature of the TSD design, the elements can represent sections of a heat exchanger or discrete modules making up the overall unit.



The major difference between the receiver and TSD models is in the thermal resistance of the massive elements. The massive elements for the receiver represent the cavity walls. The resistance to heat transfer of these walls is quite low and can be safely neglected. Thus, only the fluid thermal conductance (reciprocal of resistance) need be considered in specifying the overall thermal resistance. This is not the case for the TSD, however. The massive PCM can represent a significant resistance to heat transfer and must be considered along with the fluid thermal conductance (convective coupling strength).

The PCM can be completely solid, completely liquid, or in the two-phase regime in the melting or freezing mode. The resistance calculation is different for each of these conditions. It should be noted that each PCM element is considered a separate entity; i.e., each has its own temperature and phase boundary location. To account for the most general TSD design, longitudinal conduction between adjacent PCM elements is not included.

For the case of the PCM either completely solid or in the two-phase regime in the freezing mode (solid PCM in contact with the cycle fluid), the resistance,  $R$ , is given by the usual expression

$$R = \frac{l}{kA} \quad (17)$$

where  $l$  = the resistive path length

$k$  = the PCM solid thermal conductivity

and  $A$  = the mean heat transfer area

However, if PCM liquid is in contact with the cycle fluid (either PCM completely melted or two-phase in the melting mode), heat can also be transferred through the PCM layer by natural convection. The combined conductive-convective resistance is taken as

$$R = \frac{1}{hA + kA/l} \quad (18)$$

where  $h$  is the natural convection heat transfer coefficient, which is calculated from the relationships given in McAdams\* using the actual temperature differences.

The resistive path length,  $l$ , varies with the different PCM conditions. Considering the fluid and PCM elements shown in Figure A-3, it can be seen that the resistive path through the PCM extends from the fluid interface to the PCM element boundary when the PCM is in a single phase (solid or liquid). However, if the PCM is in the two-phase regime, the resistive path length extends only to the two-phase boundary. The heat transfer area,  $A$ , is a computer program input, assumed to be constant in a given run.

\*W. H. McAdams, Heat Transmission, 3rd ed., McGraw-Hill Book Co., New York, 1954, p. 172.



Using the resistances determined from Equations (17) and (18), the future solid temperatures are calculated when the PCM is in the single-phase regime by

$$T_i^{(s)}(t') = T_i^{(s)}(t) + \frac{\Delta t}{C_i} \left[ Z_i \Delta T_{LM} \right] \quad (19)$$

where  $Z$  is the overall coupling strength (or thermal conductance) given by:

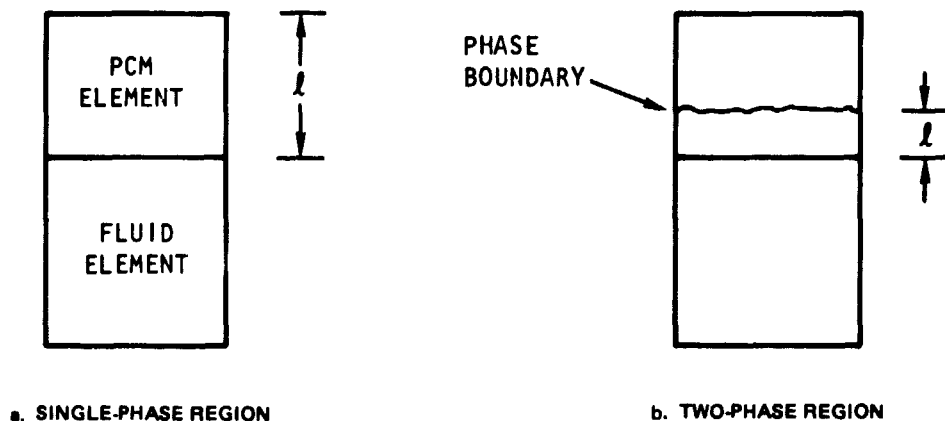
$$Z = \frac{1}{\frac{1}{H} + R} \quad (20)$$

Because longitudinal conduction is not considered, there is no conductive coupling strength term ( $K_{ij}$ ). There is no  $q_i$  term because the solar input is confined to the receiver.

If the PCM is in the two-phase regime, the massive element temperature does not change over the time interval. What does change is the location of the phase boundary (or fraction liquid). The fraction liquid,  $M$ , is given by

$$M_i(t') = M_i(t) + \frac{\Delta t}{L} \left[ Z_i \Delta T_{LM} \right] \quad (21)$$

where  $L$  is the fusion capacity of the PCM (latent heat of fusion times mass of element).



A-17538

Figure A-3. Resistive Path Length



### Temperatures of Fluids in Contact with Solids

The working fluid in contact with any of the heat transfer devices is treated as being in equilibrium with the local solid temperature. The problem is to find the steady-state outlet temperature for each fluid element, given the inlet temperature, the solid temperature, and the flow rate.

For each fluid element in a heat transfer device, an equation similar in scope and derivation to Equation (13) can be written. If  $i$  is the fluid inlet index and  $j$  is the outlet index, and contact with only one solid node is assumed, then

$$T_j^{(f)}(t^1) = T_j^{(f)}(t) + \frac{\Delta t}{C} \left[ -H\Delta T_{LM} + V(T_i^{(f)} - T_j^{(f)}) \right] \quad (22)$$

where  $C$  is the fluid element thermal capacity,  $H$  is the fluid element convective coupling strength, and  $V$  is the fluid element capacity rate. The steady-state equation is obtained by setting  $T_j^{(f)}(t^1) = T_j^{(f)}(t)$  in Equation (22) and solving the resulting expression for  $T_j^{(f)}$ . The result is

$$T_j^{(f)}(\text{steady state}) = T^{(s)} + (T_i^{(f)} - T^{(s)})e^{-H/V} \quad (23)$$

### Additional Aspects of the Calculations

The calculation around the circuit of the fluid temperatures and pressures is a major part of the evaluation of system equation closure errors. In the model, all temperature and pressure changes take place in the three heat transfer devices and the two pieces of rotating equipment. The ducts were not modeled and their outlet conditions are set equal to their inlet values. For the heat transfer devices, the fluid temperatures are calculated through the components on a node-by-node basis, using the equations previously discussed. For economy of calculation, the heat transfer component pressure drops were found simply from the inlet pressure and a given allowed fractional pressure drop.

Compressor hydrodynamic and thermodynamic performance is customarily summarized by curves of constant corrected speed,  $N_C$ , and curves of constant adiabatic efficiency,  $\eta$ , plotted on a plane with pressure ratio,  $p_r$ , on the vertical and corrected flow,  $W_C$ , on the horizontal axis. The corrected flow and speed are related to the actual flow,  $W$ , and speed,  $N_t$ , by the relations

$$W_C = W \frac{\sqrt{T/T_s}}{P/P_s} \quad (24)$$

$$N_C = N_t / \sqrt{T/T_s} \quad (25)$$

where  $T$  and  $P$  are the inlet temperature and pressure, respectively. The subscript  $s$  refers to standard conditions (70°F and 1 atm).



Map reading is complicated by the fact that the speed lines tend to drop off sharply and the efficiency contours form closed loops. The situation is greatly improved by presenting the performance information in a different manner. The maps are transformed by first constructing a set of lines that cut across the speed lines. These are labeled by values of a map parameter,  $X$ . It is convenient to let the surge line be the  $X=0$  line; negative  $X$  values then provide an indication that the compressor is in surge. Each speed line can then be converted into two curves, one of  $W_C$  vs  $X$  and one of  $p_r$  vs  $X$ . These curves represent well-behaved, single-valued functions of  $X$  that span the whole  $X$  range chosen. Knowledge of  $W_C$  and  $N_C$  thus determines  $X$ , which is then used to determine  $p_r$ . Also, from the intersection of the efficiency lines with the speed lines,  $\eta$  vs  $W_C$  curves result that then can be converted into  $\eta$  vs  $X$  curves, using the previously determined  $W_C$  vs  $X$  relation. These curves are used to find the temperature rise across the compressor. The  $\eta$  vs  $X$  curves are easier to use than the  $\eta$  vs  $W_C$  curves because the former consist of a set of essentially superimposed curves, each extending across the whole range of  $X$ , while the latter curves each cover a different, limited range of  $W_C$ .

The turbine performance is given by curves of  $W_C$  vs  $p_r$  for different corrected speeds. These lines also drop sharply. Again, by constructing map parameter lines that cut across the speed curves, two sets of well-behaved curves ( $W_C$  vs  $X$  and  $p_r$  vs  $X$ ) can be produced. The speed and flow then determine  $X$ , which, in turn, gives  $p_r$ . The efficiency can then be determined from a map consisting of curves of  $\eta$  vs  $N_C$  for different  $p_r$  values.

The outlet temperature of the compressor and turbine is calculated from the usual expression for adiabatic compression and expansion given below.

$$\text{Compression: } T_{\text{out}} = T_{\text{in}} [1 - (1/\eta)(1 - p_r^\theta)] \quad (26)$$

$$\text{Expansion: } T_{\text{out}} = T_{\text{in}} [1 - \eta(1 - 1/p_r^\theta)] \quad (27)$$

where

$$\theta = (\gamma - 1)/\gamma$$

$\gamma$  = ratio of specific heat at constant pressure to specific heat at constant volume

In these expressions, the pressure ratio,  $p_r$ , is the ratio of the outlet-to-inlet pressure for the compressor and the inlet-to-outlet pressure for the turbine.

The electrical output of the engine is calculated from the working fluid net enthalpy change in going through the turbine and compressor. Losses due to mechanical and electrical inefficiencies in the bearings, gears, and generator are accounted for by constant efficiency factors.



## COMPUTER IMPLEMENTATION

### Program Structure

The program that implements the mathematical solution to the transient problem reviewed above is called SOLARBRAYTON. It is composed of a main program plus a number of subroutines. The general structure of the program showing the relationships between the subroutines is indicated in Figure A-4; Figure A-5 shows the specific component subroutine relationships. The function of each subroutine is discussed in Table A-1.

In Figure A-4, the dashed lines from S (start) to F (finish) show the overall order of the subroutine calls. The actual transient is performed by TIMES through repetitive calls to TRANS (for transient calculations on massive elements) and NEWTON (for solution to the system equations). SYSTEM defines to NEWTON the system equations that are unique to this particular system. Both TRANS and SYSTEM do the bulk of their actual calculations via calls to a number of specific component subroutines. This modular construction of the program makes it easier to produce error-free code, facilitates program maintenance, and allows modifications to be made quickly and reliably.

Figures A-6 and A-7 are flowcharts of MAIN and TIMES, respectively, showing further details of the overall program logic.

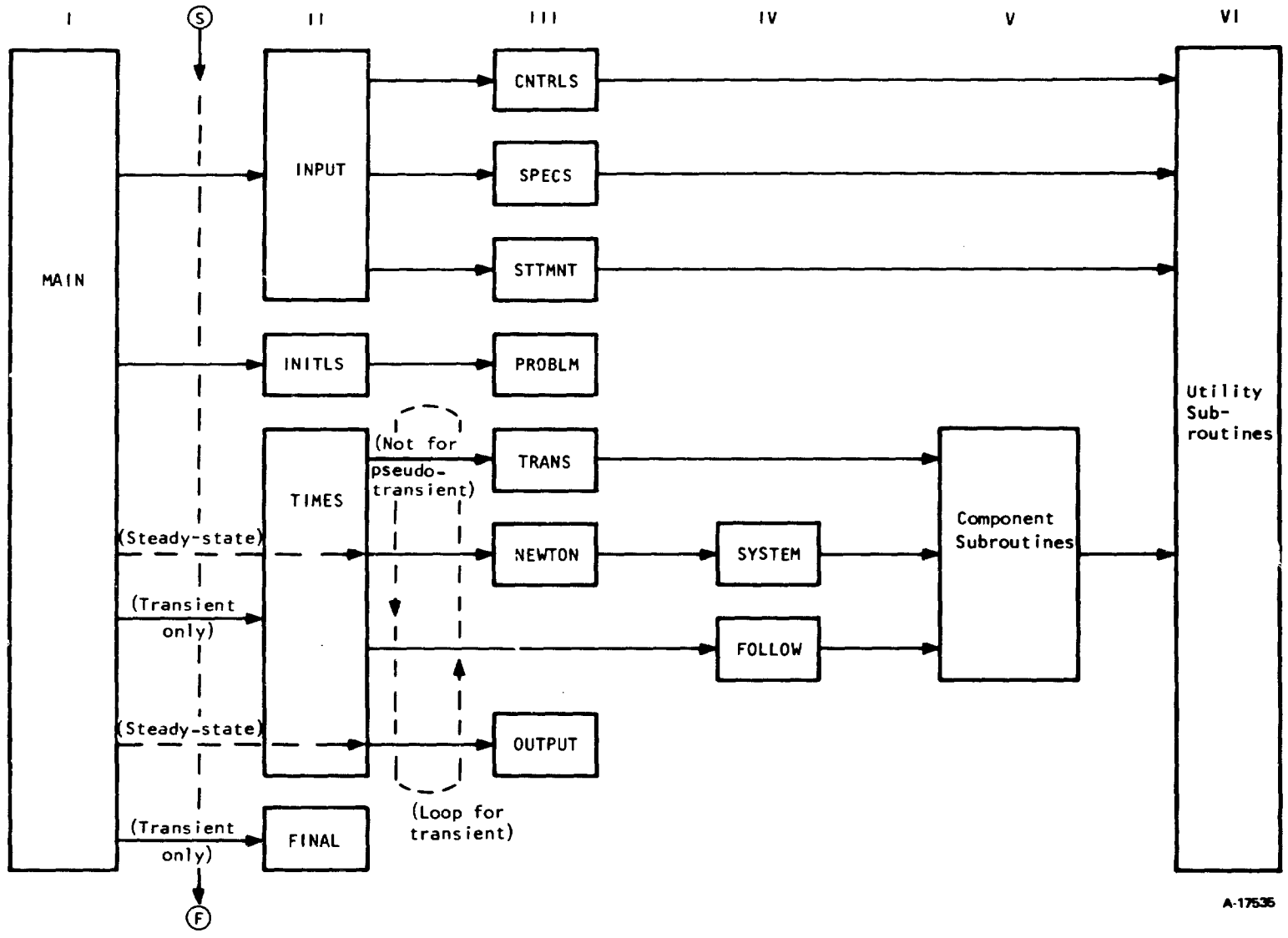
### Input Requirements

Three types of input are required by SOLARBRAYTON. These are read in by subroutines CNTRLS, SPECS, and STTMNT under the control of subroutine INPUT and are referred to as Type 1, Type 2, and Type 3 inputs, respectively. The option exists to define all of the Type 2 input by a block data subroutine and to bypass SPECS. For multiple cases in one run, only the Type 3 input is changed for the additional cases.

Type 1 input consists of program mode and run controls. It contains: indices that select various program mode, modeling, map reading, and output options; time-stepping controls for the transient; and iteration limits and convergence criteria for the internal iterative techniques. These quantities need to be reviewed and possibly changed for each new run.

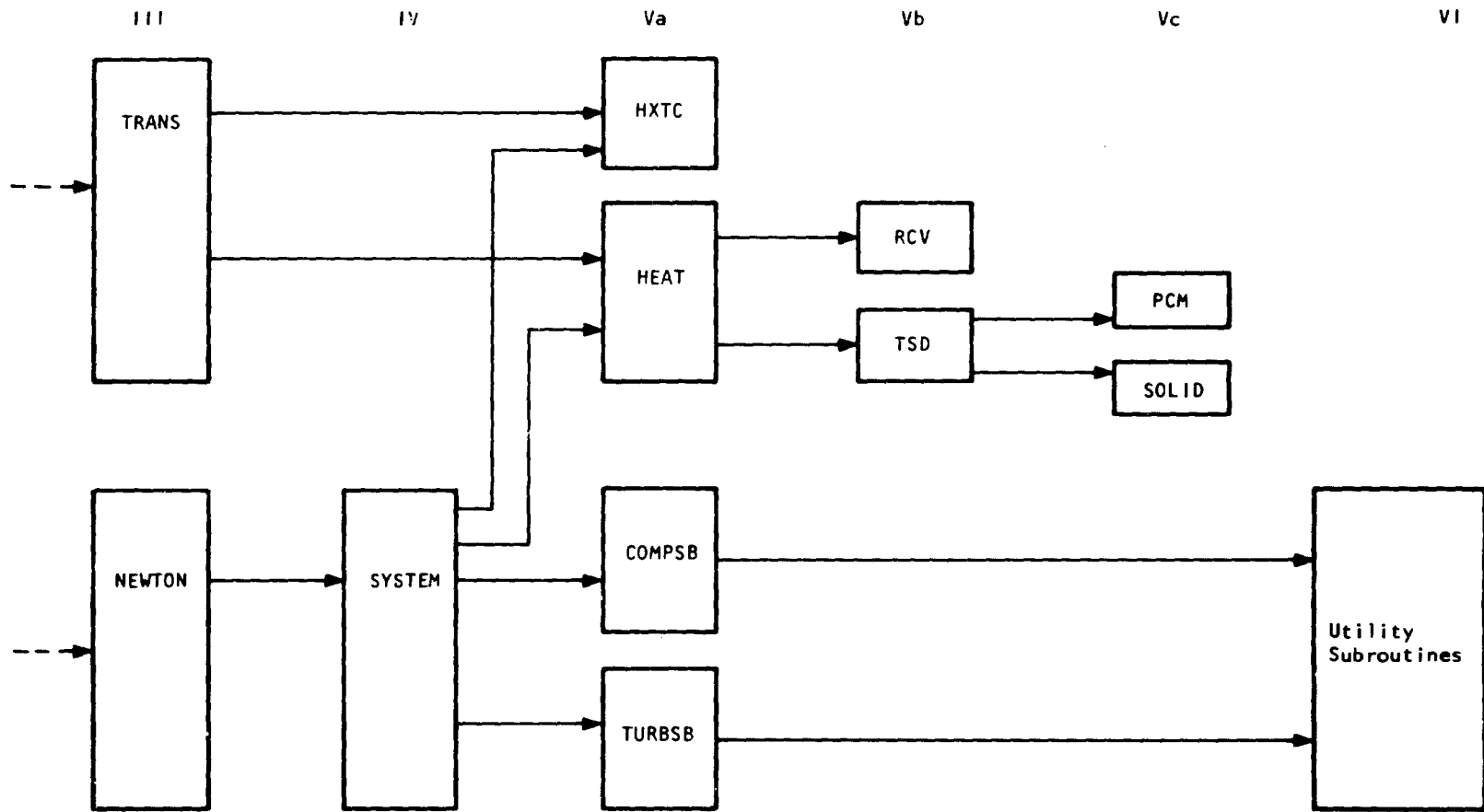
Type 2 input contains all the system and component specifications. This rather large block of data needs changing only if the system is changed or the performance specifications are updated. It is usually read directly from a data file rather than from cards.

Type 3 input constitutes the particular problem statement for the case under study and therefore changes in at least some part from case to case. Included here are indices that choose from a set of candidate variables and equations (built into SYSTEM) those that will be the  $\{x^{(j)}\}$  and the  $\{f^{(i)}\}$  for the present case. Initial estimates of the  $\{x^{(j)}\}$  needed by the Newton procedure for the solution of the system equations are also provided. High and low limits (fences) for each  $x^{(j)}$  are provided to help the iterative technique converge smoothly. Parameters required by the control logic and



A-17535

Figure A-4. SOLARBRYTON Subroutines Hierarchy Structure



A-17536

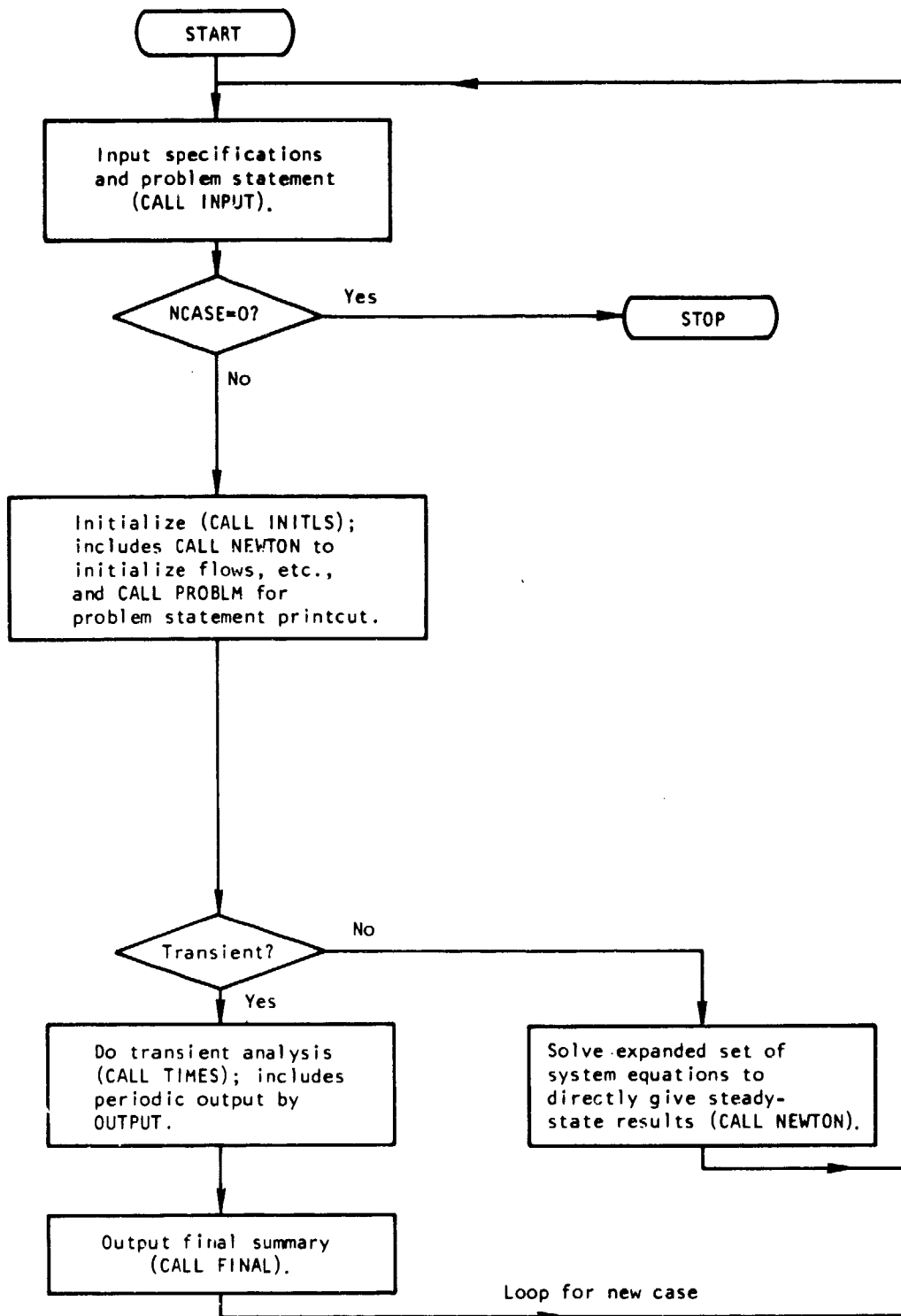
Figure A-5. Hierarchy Details for SOLARBRAYTON Component Subroutines

TABLE A-1

SUBROUTINE IDENTIFICATION LIST FOR SOLARBRAYTON  
TRANSIENT PERFORMANCE PROGRAM

LEVEL I	
MAIN	Main program that calls the four Level II subroutines.
LEVEL II	
INPUT	Master input subroutine that calls CNTRLS, SPECS, and STTMNT for actual input.
INITLS	Subroutine that performs any required initialization calculations.
TIMES	Master control program for the transient performance calculation; it increments the time and repetitively calls TRANS, NEWTON, FOLLOW, and OUTPUT.
FINAL	Produces a final summary output of the run.
LEVEL III	
CNTRLS	Inputs the program and run controls.
SPECS	Inputs the system and component specifications.
STTMNT	Inputs the problem statement, and may contain information for more than one case.
PROBLM	Subroutine to print out a problem statement page.
TRANS	Does the true transient calculations for the massive components by calling the appropriate component subroutines.
NEWTON	Solves sets of simultaneous nonlinear equations. These determine the values of those variables in equilibrium with the massive element temperatures and the boundary conditions.
OUTPUT	Produces a detailed output on a user-defined frequency basis. A one-line output is usually produced by TIMES on a more frequent basis.
LEVEL IV	
SYSTEM	Does system performance calculations that define to NEWTON the simultaneous equations that need to be solved.
FOLLOW	Does additional performance calculations not needed by NEWTON.
LEVEL V	
COMPSB	Compressor performance.
TURBSB	Turbine performance.
HXTC	Recuperator performance.
HEAT	Heat source performance; calls RCV and TSD.
RCV	Receiver performance.
TSD	Thermal storage device performance; calls POM and SOLID.
POM	Calculates resistance of TSD elements.
SOLID	Determines status of POM in each element.
LEVEL VI	
TABIN	Reads in tables.
MAPIN	Reads in maps.
READ	Reads performance from maps.
TABLE	Reads tables.
TABLE2	Special version of TABLE for schedules
HSTGRM	Special version of TABLE for histograms.

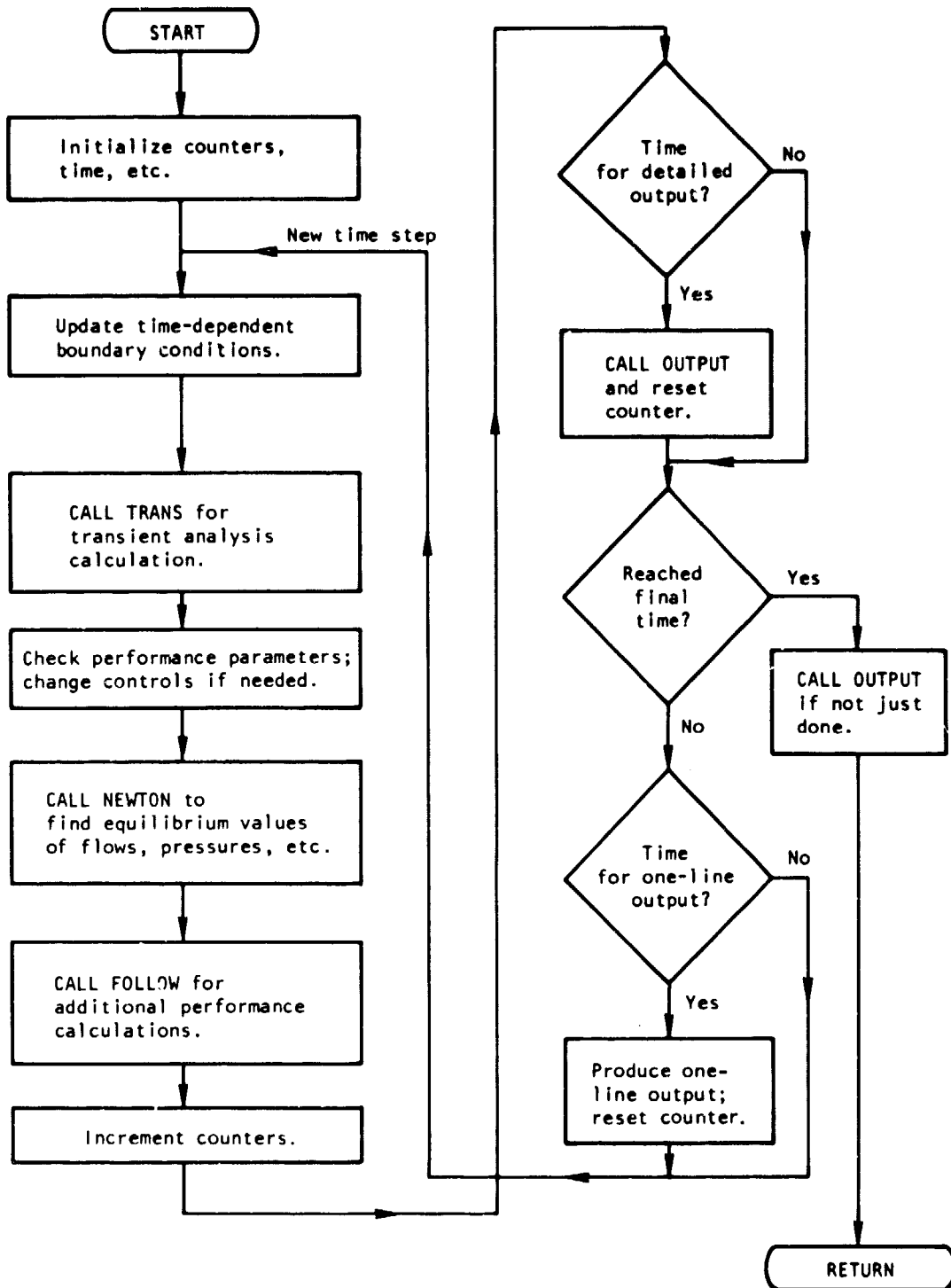




A-17541

Figure A-6. Flowchart for MAIN





A-17642

Figure A-7. Flowchart for TIMES



any values needed for individual performance indicators are specified in this block of input. Boundary conditions, both constant and time-dependent, are given, including the solar insolation for the day. This latter item is usually input directly from a data file.

### Sample Output

An example of the output of the SOLARBRAYTON performance program is presented in Figures A-8 and A-9. Figure A-8 is an example of the detailed, one-page output, printed at a particular specified time. The top of the page shows pressures (psi) and temperatures ( $^{\circ}$ R) at the various system station points (see Figure A-1).

Next are the compressor and turbine operating conditions. The scaled corrected speed, used for map reading convenience, is the ratio of the corrected speed to a reference corrected speed (80,000 rpm for the compressor and 39,434 rpm for the turbine).

This is followed by the nodal temperatures of the massive elements of the recuperator, receiver, and TSD. The fraction of liquid PCM for each TSD element is also calculated. Elements with liquid fractions between 0 and 1 are always at the PCM melting point, in this case  $1932^{\circ}$ R (NaCl). The final entry is the power output.

Figure A-9 shows a series of one-line outputs at specified time intervals. The flows and temperatures are the station values indicated in Figure A-1. SUNINS is the input value of the insolation in watts/square meter, QFLUID is the heat absorbed by the fluid in kilowatts, and POWERE is the power output in kilowatts.

### Plotting Capabilities

A computer plotting subroutine has been written and coordinated with SOLARBRAYTON. The subroutine has the capability of plotting any specified parameters as functions of time. Plots of the key variables for several runs are presented in Section 4 of this report.

## COMPONENT SPECIFICATIONS

### Rotating Equipment

The Mod "0" turbomachinery consists of a turbine and compressor (specified as GTP 36-51) and a 400-Hz generator. Performance maps for the turbine and compressor were obtained from the Garrett Turbine Engine Company and are reproduced in Appendix B. The maps are plotted in terms of pressure ratio, corrected flow, percent corrected speed, and efficiency. The actual turbomachinery operating conditions, as derived from the maps, are used to determine the cycle state points.

In accordance with usual practice, some of the flow from the compressor outlet (taken as 2 percent) is used to cool the bearings. This flow is assumed to be added to the turbine exit flow. Thus, the turbine flow is always taken as 2 percent less than the compressor flow.



PERFORMANCE RESULTS FOR CASE NO. 1 AT 12.440 HOURS

INDEX	PSIATN	PISIAL	ISIAIN	STATION I.D.
1	14.700	14.700	530.000	WORKING FLUID INLET
2	14.700	14.700	530.000	COMPRESSOR INLET
3	35.363	35.363	725.720	COMPRESSOR OUTLET
4	35.363	35.363	725.720	HX COLD SIDE INLET
5	35.010	35.010	1578.230	HX COLD SIDE OUTLET
6	35.010	35.010	1578.230	HEAT SOURCE INLET
7	33.280	33.280	1935.925	HEAT SOURCE OUTLET
8	33.280	33.280	1935.925	TURBINE INLET
9	15.165	15.165	1632.593	TURBINE OUTLET
10	15.165	15.165	1632.593	HX WARM SIDE INLET
11	14.710	14.710	805.014	HX WARM SIDE OUTLET
12	14.710	14.710	805.014	WORKING FLUID EXIT
13	15.165	15.165	1632.593	HX DUCT INLET
14	.000	.000	.000	
15	.000	.000	1960.007	RECEIVER OUTLET
16	.000	.000	1935.925	ISB OUTFLET
17	.000	.000	.000	
18	.000	.000	.000	
19	.000	.000	.000	
20	.000	.000	.000	

	SPEED	CORRECTED SPEED	SCALED CORRECTED SPEED	FLOW	CORRECTED FLOW	SCALED CORRECTED FLOW	PRESSURE RATIO	SCALED PRESSURE RATIO	EFFICIENCY	SCALED EFFICIENCY	MAP PARAMETER
COMPRESSOR	57357.	57357.	.71696	.56378	.56378	.56378	2.4057	2.4057	.77296	.77296	3.7190
TURBINE	57357.	30011.	.76228	.55192	.46593	.46593	2.1945	2.1945	.82578	.82578	4.1151

SPEEDS ARE IN RPM  
 FLOWS ARE IN LHM/SEC. COMPRESSOR FLOW IS INLET, TURBINE FLOW IS INLET

RECUPERATOR PARAMETERS		EFFECTIVENESS = .9401				NITRGEN USED = 1				
INTERNAL TEMPERATURES										
1591.	1565.	1538.	1510.	1482.	1453.	1424.	1394.	1363.	1333.	
1301.	1269.	1236.	1213.	1169.	1134.	1099.	1063.	1026.	988.9	
950.7	911.8	872.0	831.5	791.5						
RECEIVER PARAMETERS		EFFECTIVENESS = .9401				NITRGEN USED = 1				
INTERNAL TEMPERATURES										
1721.	1760.	1799.	1837.	1875.	1913.	1951.	1989.	2027.	2064.	
THERMAL STORAGE PARAMETERS		EFFECTIVENESS = .9401				NITRGEN USED = 1				
INTERNAL TEMPERATURES										
1960.	1957.	1932.	1932.	1932.	1932.	1932.	1932.	1932.	1932.	
FRACTION LIQUID										
1.000	1.000	.9093	.7997	.5533	.4307	.3345	.2540	.2000	.1538	
ELECTRICAL OUTPUT POWER =		13.61 KW								

Figure A-8. Sample Detailed Output



AIRESEARCH MANUFACTURING COMPANY

TIME	SUMINS	OFLUID	POWER	WFSO	W(3)	T(4)	T(8)	T(13)	T(15)	T(15)	NR07
12.440	832.000	54.412	13.404	.552	.552	1578.23	1935.92	1432.59	1940.01	1935.92	57357.08
12.444	832.000	54.418	13.407	.552	.552	1578.19	1935.93	1432.59	1959.99	1935.93	57357.08
12.448	832.000	54.422	13.407	.552	.552	1578.16	1935.93	1432.60	1959.97	1935.93	57357.08
12.452	835.000	54.430	13.407	.552	.552	1578.15	1935.97	1432.63	1940.30	1935.97	57357.08
12.457	835.000	54.434	13.408	.552	.552	1578.14	1936.00	1432.66	1960.57	1936.00	57357.08
12.461	835.000	54.440	13.408	.552	.552	1578.14	1936.02	1432.68	1940.77	1936.02	57357.08
12.465	829.000	54.439	13.408	.552	.552	1578.14	1936.01	1432.67	1960.68	1936.01	57357.08
12.469	829.000	54.433	13.407	.552	.552	1578.12	1935.96	1432.62	1940.12	1935.96	57357.08
12.473	829.000	54.430	13.406	.552	.552	1578.09	1935.91	1432.58	1959.65	1935.91	57357.08
12.477	829.000	54.429	13.406	.552	.552	1578.07	1935.88	1432.55	1959.28	1935.88	57357.08
12.482	829.000	54.424	13.407	.550	.550	1578.08	1935.85	1433.17	1959.24	1935.85	57256.10
12.486	829.000	54.431	13.407	.550	.550	1578.33	1935.88	1433.19	1959.31	1935.88	57256.10
12.490	829.000	54.421	13.407	.550	.550	1578.42	1935.89	1433.20	1959.42	1935.89	57256.10
12.494	829.000	54.414	13.407	.550	.550	1578.44	1935.91	1433.21	1959.53	1935.91	57256.10
12.498	829.000	54.413	13.407	.550	.550	1578.50	1935.92	1433.23	1959.63	1935.92	57256.10
12.502	830.000	54.412	13.407	.550	.550	1578.52	1935.94	1433.24	1959.80	1935.94	57256.10
12.507	830.000	54.412	13.407	.550	.550	1578.55	1935.96	1433.26	1959.98	1935.96	57256.10
12.511	830.000	54.412	13.407	.550	.550	1578.57	1935.98	1433.28	1940.12	1935.98	57256.10
12.515	830.000	54.411	13.407	.550	.550	1578.58	1935.99	1433.29	1940.23	1935.99	57256.10
12.519	830.000	54.410	13.407	.550	.550	1578.60	1936.00	1433.30	1940.31	1936.00	57256.10
12.523	830.000	54.410	13.407	.550	.550	1578.61	1936.01	1433.31	1940.37	1936.01	57256.10
12.527	830.000	54.409	13.407	.550	.550	1578.63	1936.02	1433.31	1940.41	1936.02	57256.10
12.532	818.000	54.401	13.407	.550	.550	1578.64	1935.97	1433.27	1959.96	1935.97	57256.10
12.536	818.000	54.133	13.403	.548	.548	1578.67	1935.84	1434.39	1959.02	1935.84	57119.04
12.540	818.000	53.417	13.273	.544	.544	1579.60	1935.85	1434.53	1959.19	1935.85	56904.57
12.544	818.000	53.504	13.273	.544	.544	1580.41	1935.90	1434.57	1959.44	1935.90	56904.57
12.548	818.000	53.459	13.274	.544	.544	1580.76	1935.94	1434.60	1959.88	1935.94	56904.57
12.552	824.000	53.429	13.314	.544	.544	1580.95	1936.08	1434.00	1940.86	1936.08	57018.44
12.557	824.000	54.110	13.505	.550	.550	1580.39	1936.10	1433.90	1940.88	1936.10	57241.23
12.561	824.000	54.203	13.505	.550	.550	1579.74	1936.08	1433.88	1940.85	1936.08	57241.23
12.565	824.000	54.233	13.505	.550	.550	1579.54	1936.07	1433.87	1940.73	1936.07	57241.23
12.569	824.000	54.247	13.504	.550	.550	1579.43	1936.06	1433.86	1940.55	1936.06	57241.23
12.573	824.000	54.255	13.504	.550	.550	1579.34	1936.04	1433.84	1940.36	1936.04	57241.23
12.577	824.000	54.260	13.504	.550	.550	1579.31	1936.02	1433.83	1940.19	1936.02	57241.23
12.582	824.000	54.263	13.504	.550	.550	1579.28	1936.01	1433.82	1940.04	1936.01	57241.23
12.586	823.000	54.261	13.503	.550	.550	1579.24	1935.96	1433.78	1959.57	1935.96	57241.23
12.590	823.000	54.260	13.502	.550	.550	1579.21	1935.92	1433.74	1959.18	1935.92	57241.23
12.594	823.000	54.078	13.470	.548	.548	1579.34	1935.92	1434.38	1959.22	1935.92	57137.46
12.598	822.000	54.054	13.470	.548	.548	1579.51	1935.92	1434.38	1959.22	1935.92	57137.46
12.602	822.000	54.044	13.470	.548	.548	1579.57	1935.92	1434.37	1959.18	1935.92	57137.46
12.607	822.000	54.042	13.470	.548	.548	1579.60	1935.92	1434.37	1959.17	1935.92	57137.46
12.611	822.000	54.039	13.470	.548	.548	1579.62	1935.92	1434.38	1959.18	1935.92	57137.46
12.615	822.000	54.037	13.470	.548	.548	1579.64	1935.93	1434.38	1959.20	1935.93	57137.46
12.619	825.000	54.040	13.470	.548	.548	1579.66	1935.97	1434.41	1959.57	1935.97	57137.46
12.623	825.000	54.042	13.471	.548	.548	1579.68	1936.00	1434.45	1959.88	1936.00	57137.46
12.627	825.000	54.043	13.471	.548	.548	1579.70	1936.03	1434.47	1940.13	1936.03	57137.46
12.632	825.000	54.043	13.472	.548	.548	1579.73	1936.05	1434.49	1940.32	1936.05	57137.46
12.636	827.000	54.044	13.472	.548	.548	1579.75	1936.09	1434.53	1940.49	1936.09	57137.46

Figure A-9. Sample One-Line Output

A-1777

Because the turbine and compressor are attached to the same shaft, the rotating speeds are assumed to be the same for each component. Since the efficiency and flow rate are strongly dependent on rotating speed, only a narrow range of speeds is reasonable for the turbomachinery. Indeed, the speed is restricted to values between 53,000 and 62,500 rpm during engine operation.

The generator is not explicitly modeled in the computer program. An efficiency of 88 percent is assumed for this component. Additional mechanical and gearbox losses are accounted for by assuming a rotating efficiency of 91 percent. These efficiencies, which are, of course, in addition to the turbine and compressor efficiencies, are applied to the net power produced, i.e., the difference between the power of the turbine and the power of the compressor.

### Recuperator

The proposed recuperator for the Mod "0" engine consists of an existing design used in the GT601 engine. Two heat exchanger cores are required. The heat exchangers are made of stainless steel and have an estimated weight of 400 lb. The weight includes that of the cores and manifolds and also any associated ducting not otherwise accounted for.

For use in the computer program, the recuperator is specified by curve-fits of hot- and cold-side thermal conductance data as functions of flow rate and temperature. The data were generated by AIRsearch from a detailed computer representation of the recuperator. For the hot side

$$H = 0.1017 T^{0.567} W^{0.316} \quad (28)$$

and for the cold side

$$H = 0.08214 T^{0.579} W^{0.289} \quad (29)$$

where  $H$  is the thermal conductance, Btu/sec-°R

$T$  is the average fluid temperature, °R

and  $W$  is the flow rate, lb/sec

The values calculated from Equations (28) and (29) are applied to the recuperator finite elements (see Equation (13)) and used to determine recuperator performance. The recuperator pressure drops are taken as 3 percent of the inlet pressure for the hot side and 1 percent of the inlet pressure for the cold side. These are the design points for the Mod "0" engine cycle.

The 2-percent compressor flow that is used to cool the bearings bypasses the cold side of the recuperator. Thus the hot-side flow is always 2 percent greater than the cold-side flow.



## Receiver

The receiver configuration is that of the AiResearch ABSR Phase II design. The receiver is constructed of Inconel 625 and has a weight of 80 lb (heat exchanger only). The thermal conductance is specified by the following relationship generated by AiResearch from a detailed computer model of the receiver:

$$H = 0.1051 T^{0.222} W^{0.288} \quad (30)$$

The temperature dependence of the receiver differs from that of the recuperator because of changes in the temperature dependence of air thermophysical properties at the elevated receiver temperature. It should be noted that only one thermal conductance equation is required, because the receiver is a one-fluid heat exchanger, modeled as a fluid and a solid wall.

The thermal conductance values calculated from Equation (30) are applied to the receiver finite elements (see Equation (16)) by the computer program and used to determine receiver performance. The receiver pressure drop is taken as 3 percent of the inlet pressure, which is the approximate receiver pressure drop at design flow (0.6 lb/sec). Because of compressor flow bypassed to cool the bearings, the flow through the receiver is 2 percent less than the flow through the compressor.

## Thermal Storage Device

The thermal storage device is the one major component in the Brayton engine that does not have an existing design; part of the present study effort is to establish a preliminary or conceptual design for the TSD. Indeed, in running the computer program, various sizes and materials for the TSD are required. Thus, the TSD component specification changes for each run.

Heat of fusion TSD's can perhaps be divided into two classifications--integral with the receiver and separate from the receiver. A possible schematic for an integral thermal storage system is shown in Figure A-10. The storage device is actually part of the receiver, so that no additional heat exchangers, ducting, or controls are necessary. The PCM is shown contained in a heat transfer matrix that could be metallic or ceramic. The PCM is charged (melted) directly by solar insolation. Careful design would be necessary to ensure that the PCM be totally melted. This might prove to be difficult at the cold end (receiver inlet). Because the PCM is integral with the receiver, it will affect the heat transfer during normal operation by acting as additional resistance. This will tend to raise the cavity wall temperature.

A separate or nonintegral thermal storage system is shown in Figure A-11. Because the TSD is charged by the cycle air, the melting point of the PCM must be somewhat below the nominal turbine inlet temperature. In addition, the separate heat exchanger will use up some of the cycle pressure drop. Despite these limitations and the requirement for additional equipment, it is felt



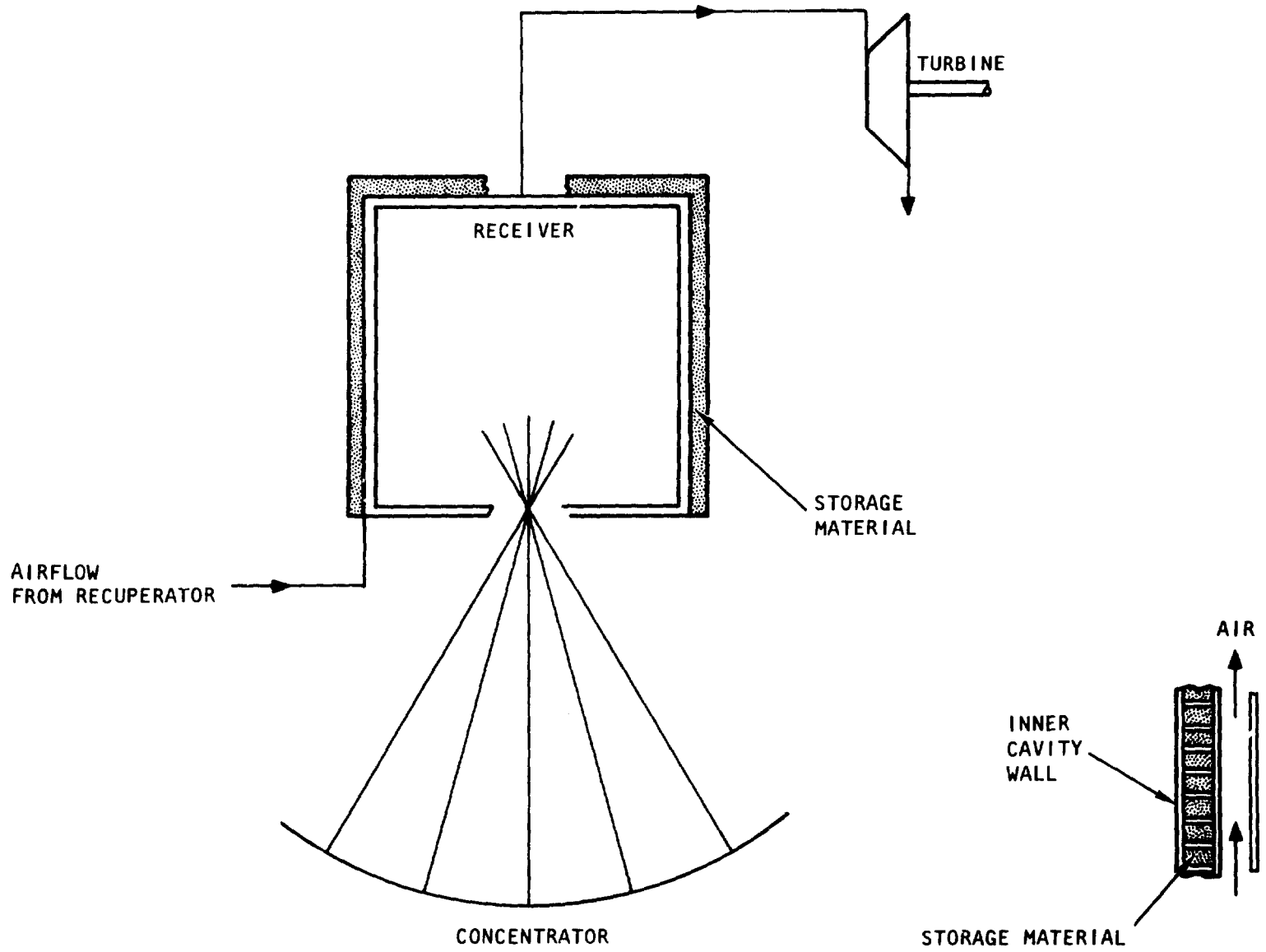


Figure A-10. Integral Thermal Storage System

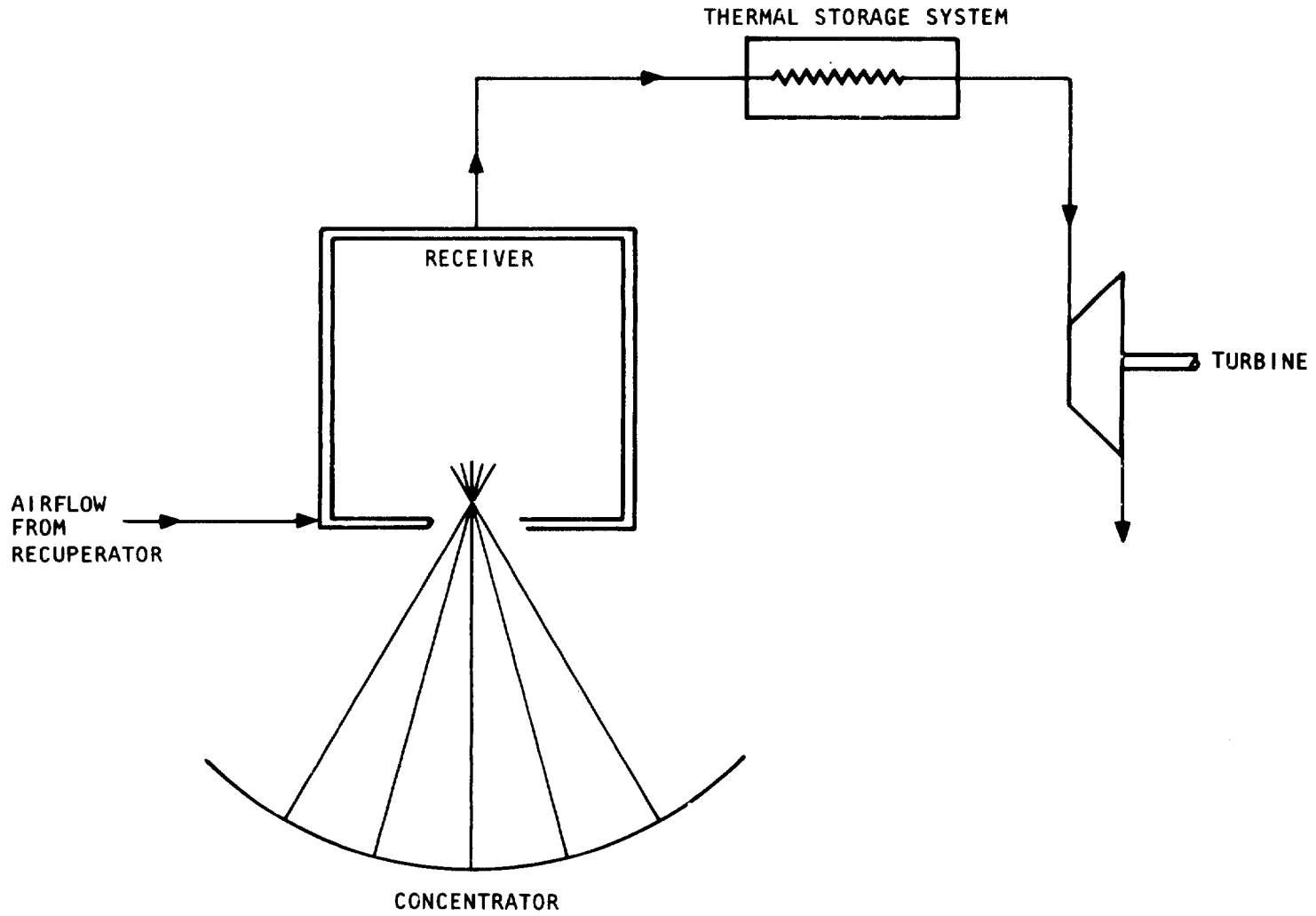


Figure A-11. Nonintegral Thermal Storage System

A-5613



that nonintegral thermal storage is the better choice, especially since the receiver for the ABSR Phase II has already been constructed. The storage device does entail some developmental and operational risk, and it would seem prudent to separate it from the receiver, while allowing for individual component optimization. The nonintegral TSD is considered exclusively in this study.

Although the TSD model is completely general, a specific configuration must be assumed to determine the specifications required to run the program. Different configurations with the same characteristics (fluid thermal conductance, PCM resistance, weight of PCM, etc.) will perform similarly, so the selection of a design for the present feasibility study is not critical. The representative configuration selected is that of a shell and tube heat exchanger. The unit consists of a bundle of hollow tubes through which the cycle fluid (air) flows. Surrounding the tubes, and filling up the shell, is the PCM. The configuration is shown schematically in Figure A-12. To study the more important variables in greater detail, a tube size of 0.25-in.-OD/0.20-in.-ID with triangular spacing on 1-in. centers has been fixed. This sets the resistive path length for single-phase PCM at 0.375 in. For the tubular configuration, the fluid thermal conductance is given by

$$H = BT^{0.268} W^{0.8} \quad (31)$$

where B is a parameter that is a function of the size of the TSD heat exchanger.

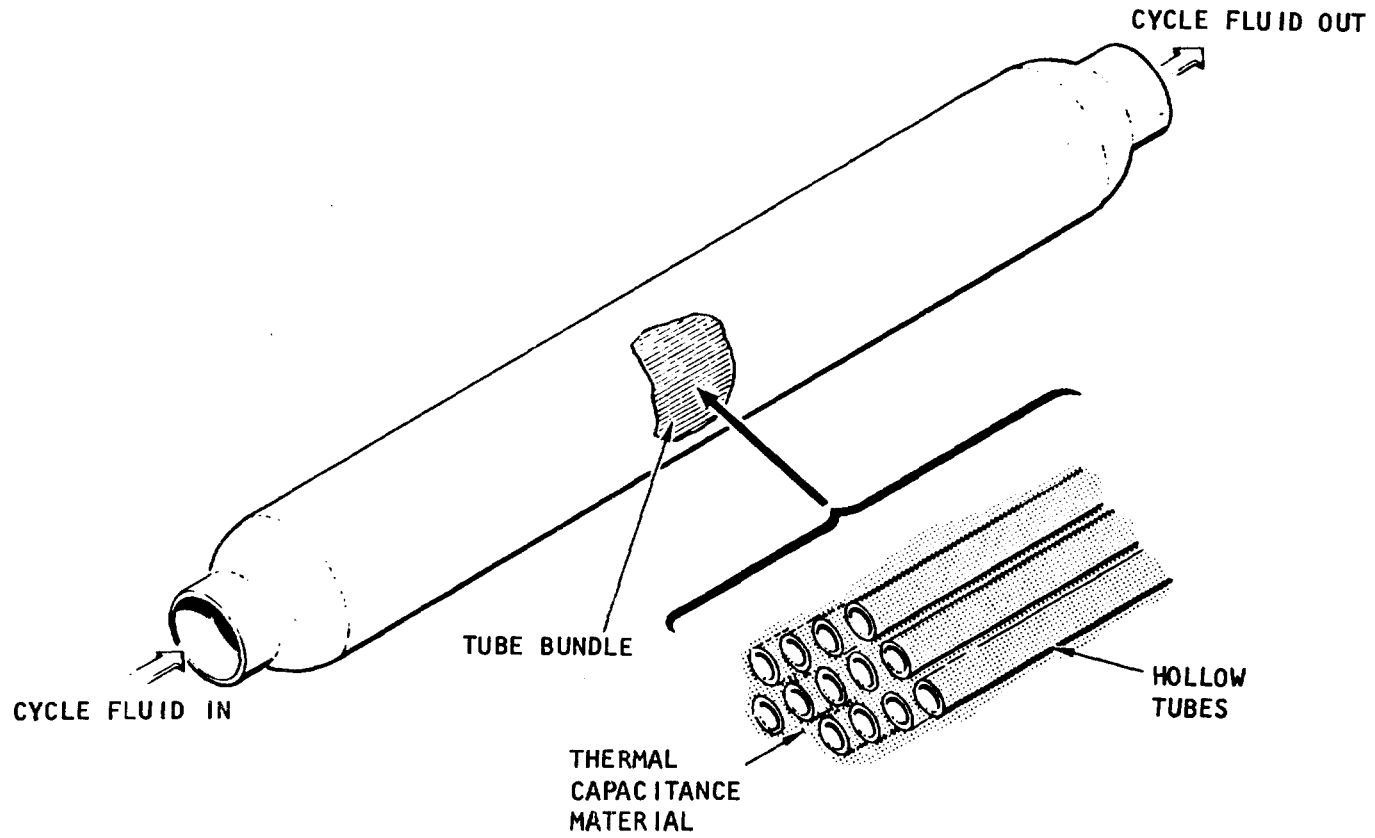
Equation (31) is a general expression for the thermal conductance of turbulent airflow inside tubes in the temperature range of the TSD.

The remaining key variables are the PCM used (and its thermophysical properties), the weight of PCM in the TSD, and the allowable pressure drop. Specifying these variables completely defines the TSD and allows for the calculation of the parameter B. The thermal conductance values calculated from Equation (31) are applied to the TSD finite elements (see Equations (19) through (21)) by the computer program and used to determine TSD performance.

For all sizes studied in the present effort, the pressure drop was taken as 2 percent of the inlet pressure for full flow through the TSD. At reduced flows, the pressure drop is reduced proportionately.

As previously mentioned, the heat exchanger walls, which physically separate the cycle fluid and the PCM, are effectively included in the PCM elements. The actual wall resistance is quite low and the weight is about 10 to 20 percent of the PCM weight.



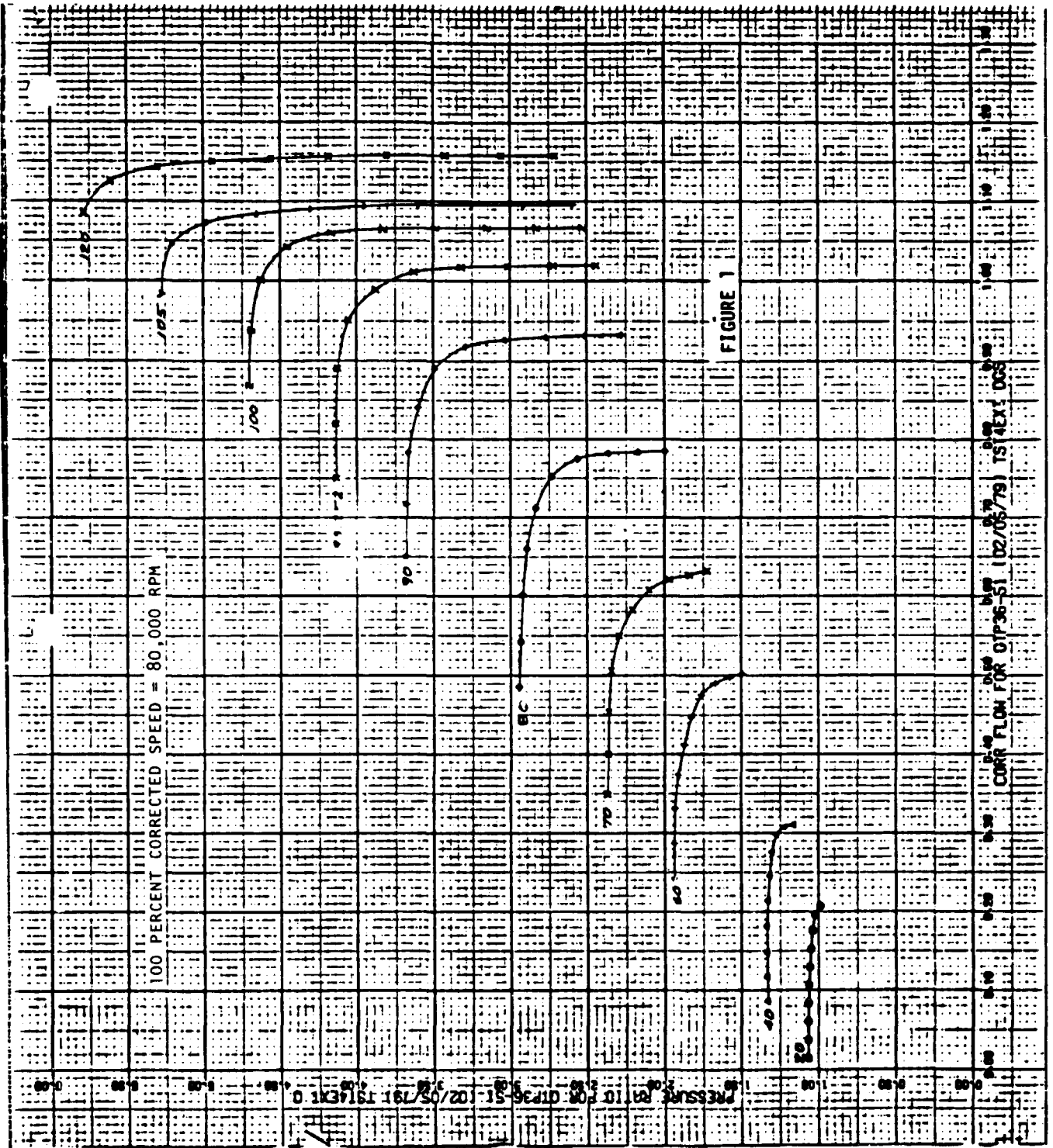


S-30294

Figure A-12. Typical Shell and Tube Heat Exchanger Arrangement for Thermal Energy Storage

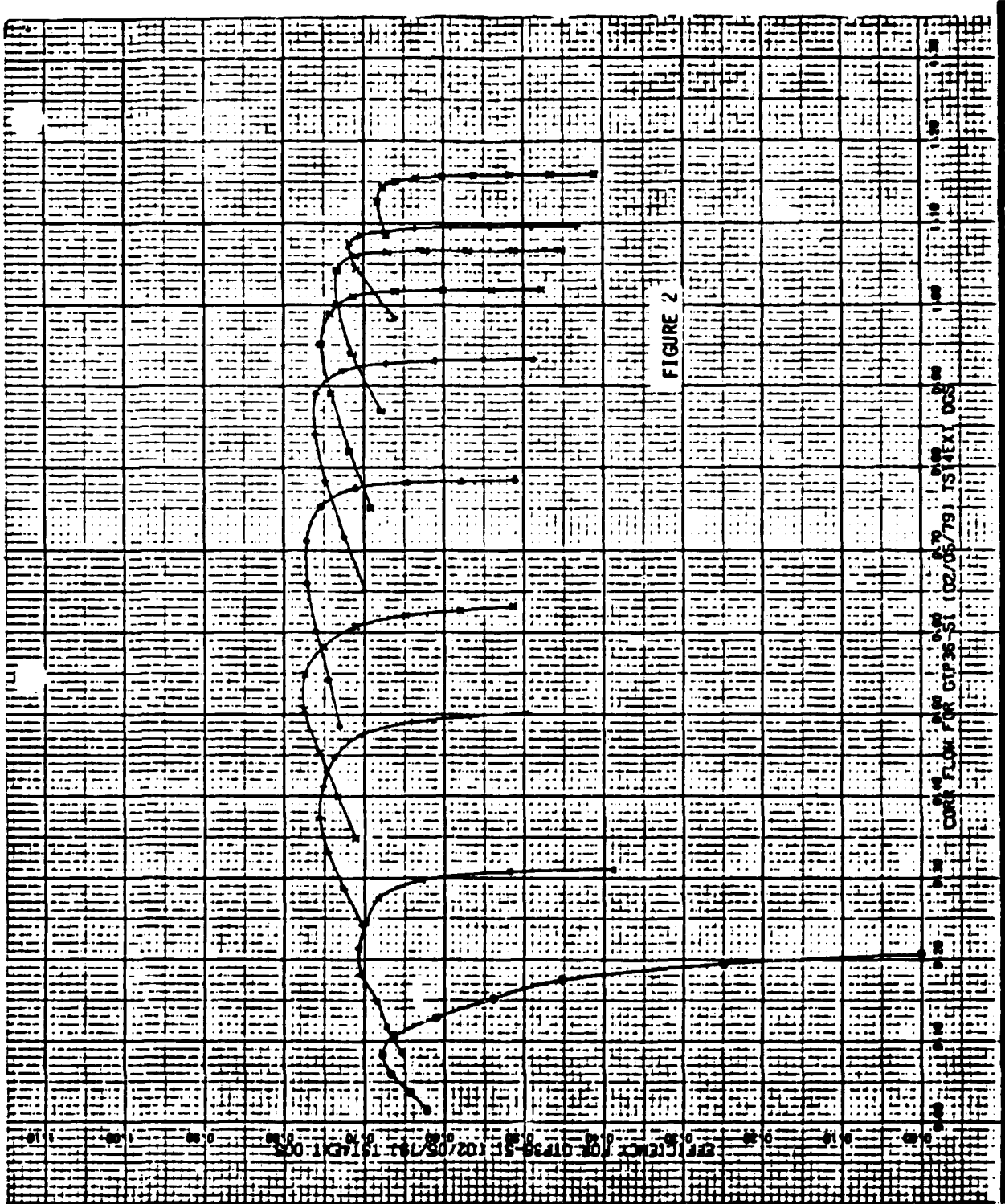
APPENDIX B  
TURBOMACHINERY PERFORMANCE MAPS

ORIGINAL ENGINE  
GOOD QUALITY

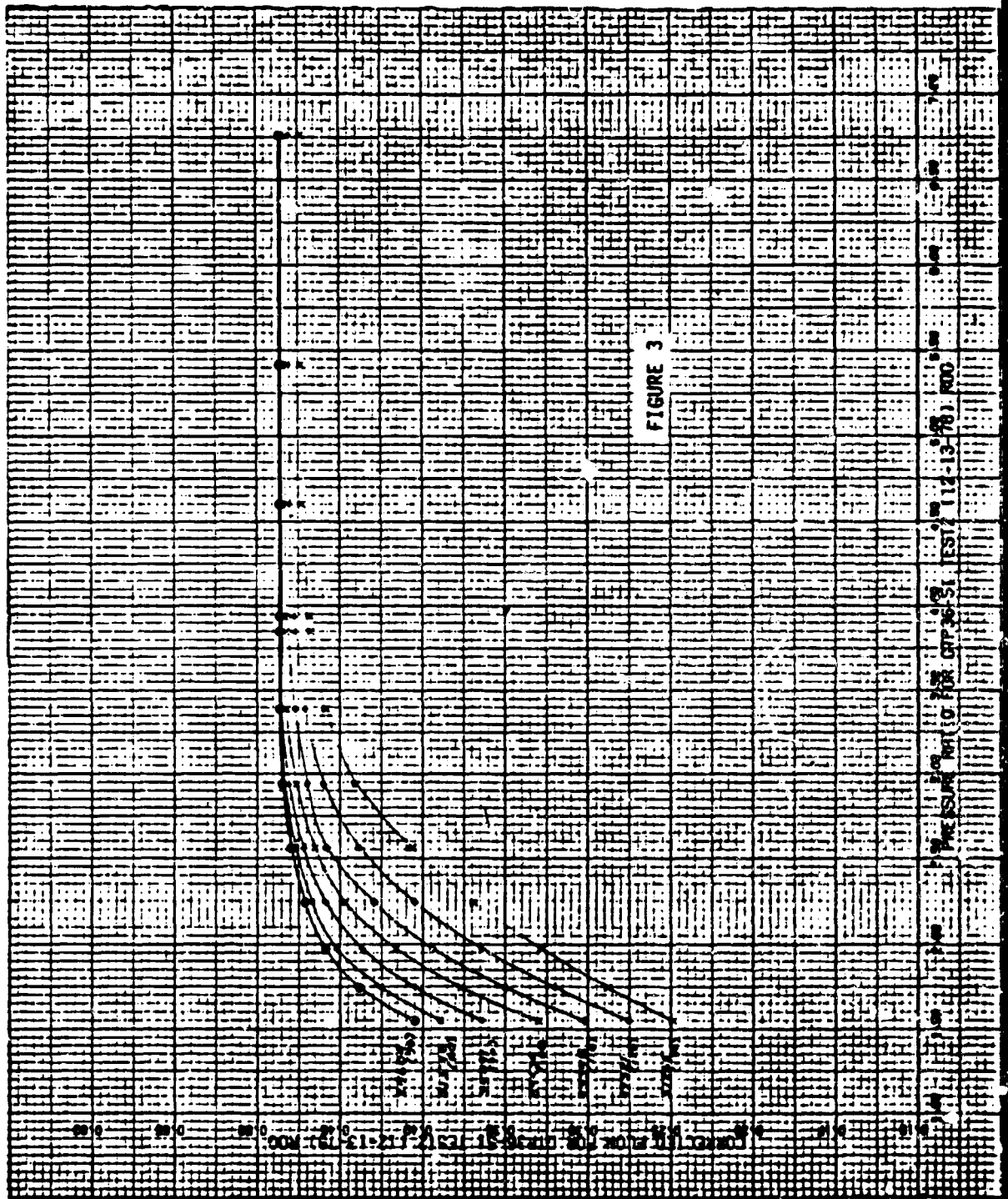


AIRESEARCH MANUFACTURING COMPANY

ORIGINAL PAGE IS  
OF POOR QUALITY



ORIGINAL PAGE IS  
OF POOR QUALITY



ORIGINAL PAGE IS  
OF POOR QUALITY

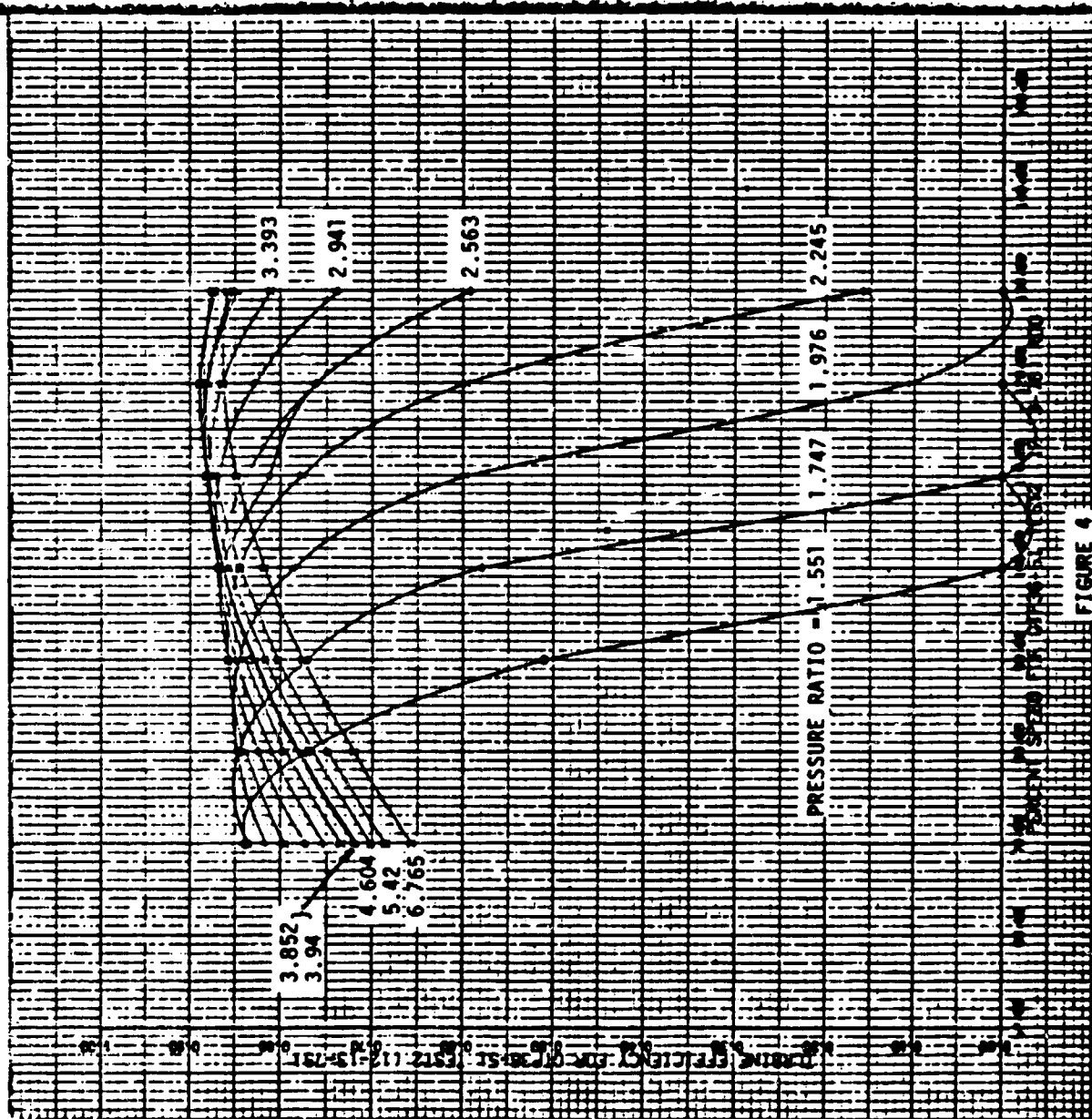


FIGURE 4

